CEREBRAL CAVERNOUS MALFORMATION

Distinct cellular roles for PDCD10 define a gut-brain axis in cerebral cavernous malformation

Alan T. Tang[1], Katie R. Sullivan[1], Courtney C. Hong[1], Lauren M. Goddard[1], Aparna Mahadevan[1], Aileen Ren[1], Heidy Pardo[2], Amy Peiper[2], Erin Griffin[2], Ceylan Tanes[3], Lisa M. Mattei[3], Jisheng Yang[1], Li Li[1], Patricia Mericko-Ishizuka[1], Le Shen[4], Nicholas Hobson[4], Romuald Girard[4], Rhonda Lightle[4], Thomas Moore[4], Robert Shenkar[4], Sean P. Polster[4], Claudia J. Roedel[5], Ning Li[6], Qin Zhu[7], Kevin J. Whitehead[8], Xiangjian Zheng[9,10], Amy Akers[11], Leslie Morrison[12], Helen Kim[13], Kyle Bittinger[3], Christopher J. Lengner[6,14,15], Markus Schwaninger[16], Anna Velcich[17], Leonard Augenlicht[17], Salim Abdelilah-Seyfried[5,18], Wang Min[19], Douglas A. Marchuk[2], Issam A. Awad[4], Mark L. Kahn[1]*

Cerebral cavernous malformation (CCM) is a genetic, cerebrovascular disease. Familial CCM is caused by genetic mutations in *KRIT1*, *CCM2*, or *PDCD10*. Disease onset is earlier and more severe in individuals with *PDCD10* mutations. Recent studies have shown that lesions arise from excess mitogen-activated protein kinase kinase kinase 3 (MEKK3) signaling downstream of Toll-like receptor 4 (TLR4) stimulation by lipopolysaccharide derived from the gut microbiome. These findings suggest a gut-brain CCM disease axis but fail to define it or explain the poor prognosis of patients with *PDCD10* mutations. Here, we demonstrate that the gut barrier is a primary determinant of CCM disease course, independent of microbiome configuration, that explains the increased severity of CCM disease associated with PDCD10 deficiency. Chemical disruption of the gut barrier with dextran sulfate sodium augments CCM formation in a mouse model, as does genetic loss of *Pdcd10*, but not *Krit1*, in gut epithelial cells. Loss of gut epithelial *Pdcd10* results in disruption of the colonic mucosal barrier. Accordingly, loss of Mucin-2 or exposure to dietary emulsifiers that reduce the mucus barrier increases CCM burden analogous to loss of *Pdcd10* in the gut epithelium. Last, we show that treatment with dexamethasone potently inhibits CCM formation in mice because of the combined effect of action at both brain endothelial cells and gut epithelial cells. These studies define a gut-brain disease axis in an experimental model of CCM in which a single gene is required for two critical components: gut epithelial function and brain endothelial signaling.

INTRODUCTION

A gut-brain axis has been implicated in a large number of diseases, including stroke (*1*, *2*), dementia (*3*), Parkinson's disease (*4*), metabolic disorders such as diabetes (*5*, *6*), and gastrointestinal diseases such as inflammatory bowel disease (*7*). Such pathogenic circuits hold the promise of treating diseases in relatively inaccessible sites such as the brain through manipulation of more accessible sites such as the gut or combining gut and brain targets for more effective therapies, but such translation requires clear definition of the pathway between organs. Numerous mechanisms have been proposed to explain connections between the gut and brain, including microbiota-generated metabolites that impact brain function, effects of the gut microbiome on local immune cells that may then travel to the brain, and direct communication between the gut and brain mediated by the nervous system or circulating factors [reviewed in (*8*–*10*)]. However, for most of these diseases, a clear molecular and cellular basis for a gut-brain axis remains elusive because of the difficulty of demonstrating cause and effect between events occurring at two different sites. Leveraging the discovery of gut-brain disease axes to new therapies requires a better understanding of such relationships.

Cerebral cavernous malformation (CCM) is a vascular disease that predominantly affects the brain and is a common cause of hemorrhagic stroke and seizure (*11*). Standard of care remains symptom management and neurosurgical resection—there remains no disease-modifying medical therapy (*12*). CCMs arise because of loss-of-function mutations in three genes, *KRIT1* [also known as (aka) *CCM1*], *CCM2*,

[1]Department of Medicine and Cardiovascular Institute, University of Pennsylvania, 3400 Civic Center Blvd, Philadelphia, PA 19104, USA. [2]Department of Molecular Genetics and Microbiology, Duke University School of Medicine, Durham, NC 27710, USA. [3]Division of Gastroenterology, Hepatology, and Nutrition, Children's Hospital of Philadelphia, Philadelphia, PA 19104, USA. [4]Neurovascular Surgery Program, Section of Neurosurgery, Department of Surgery, University of Chicago School of Medicine and Biological Sciences, Chicago, IL 60637, USA. [5]Institute for Biochemistry and Biology, Department of Animal Physiology, Potsdam University, Karl-Liebknecht-Str. 24-25, Haus 26, 14476 Potsdam, Germany. [6]Department of Biomedical Sciences, School of Veterinary Medicine, University of Pennsylvania, Philadelphia, PA 19104, USA. [7]Graduate Group in Genomics and Computational Biology, Perelman School of Medicine, University of Pennsylvania, Philadelphia, PA 19104, USA. [8]Division of Cardiovascular Medicine and the Program in Molecular Medicine, University of Utah, Salt Lake City, UT 84112, USA. [9]Department of Pharmacology, School of Basic Medical Sciences, Tianjin Medical University, Tianjin 300070, China. [10]Centenary Institute, Sydney Medical School, University of Sydney, Sydney, NSW 2050, Australia. [11]Angioma Alliance, Norfolk, VA 23517, USA. [12]Department of Neurology and Pediatrics, University of New Mexico, Albuquerque, NM 87106, USA. [13]Center for Cerebrovascular Research, Department of Anesthesia and Perioperative Care, University of California, San Francisco, San Francisco, CA 94110, USA. [14]Department of Cell and Developmental Biology, Perelman School of Medicine, University of Pennsylvania, Philadelphia, PA 19104, USA. [15]Institute for Regenerative Medicine, University of Pennsylvania, Philadelphia, PA 19104, USA. [16]Institute of Experimental and Clinical Pharmacology and Toxicology, University of Lübeck, 23562 Lübeck, Germany. [17]Department of Cell Biology, Albert Einstein College of Medicine/Albert Einstein Cancer Center, NY 10461, USA. [18]Institute of Molecular Biology, Hannover Medical School, Carl-Neuberg Str. 1, D-30625 Hannover, Germany. [19]Department of Pathology and the Vascular Biology and Therapeutics Program, Yale University School of Medicine, New Haven, CT 06510, USA.
*Corresponding author. Email: markkahn@pennmedicine.upenn.edu

and *PDCD10* (aka *CCM3*), that encode components of a single, heterotrimeric, adaptor protein complex. This "CCM complex" binds and negatively regulates the mitogen-activated protein kinase kinase kinase 3 (MEKK3 aka MAP3K3) in endothelial cells through a direct interaction between CCM2 and MEKK3 (*13*–*17*). Familial CCM disease arises because of germline, heterozygous loss of function mutations in any of the three CCM genes, but clinical studies have demonstrated that individuals with *PDCD10* mutations develop disease decades earlier than those with *KRIT1* or *CCM2* mutations and are more likely to suffer disabling brain hemorrhage and stroke (*18*, *19*). Recent studies demonstrated that lipopolysaccharide (LPS) derived from Gram-negative bacteria (GNB) in the gut microbiome drives CCM disease by activating Toll-like receptor 4 (TLR4) and MEKK3 signaling in brain endothelial cells (*20*). These findings support a gut-brain axis in CCM disease, but it remains unclear how LPS from the gut lumen reaches TLR4 receptors in the brain vasculature and which steps in this journey control pathogenesis.

In the present study, we identified the gut barrier as a critical component of the CCM gut-brain axis that bridges the intestinal microbiome and the brain endothelium during disease pathogenesis. We demonstrated that programmed cell death protein 10 (PDCD10)–dependent changes in the colonic gut barrier underlie the clinical observation that germline heterozygosity of *PDCD10* confers a more severe form of CCM disease than germline heterozygosity of *KRIT1* or *CCM2*. We also found that chronic oral intake of P80, a dietary emulsifier present in preserved foods, disrupts the mucus barrier and accelerates CCM formation in a preclinical mouse disease model without altering the gut microbiome. Last, we demonstrated that dexamethasone potently blocked CCM formation in mice because of dual effects in brain endothelial cells and gut epithelial cells, highlighting the translational value of defining a gut-brain disease axis at the molecular and cellular levels.

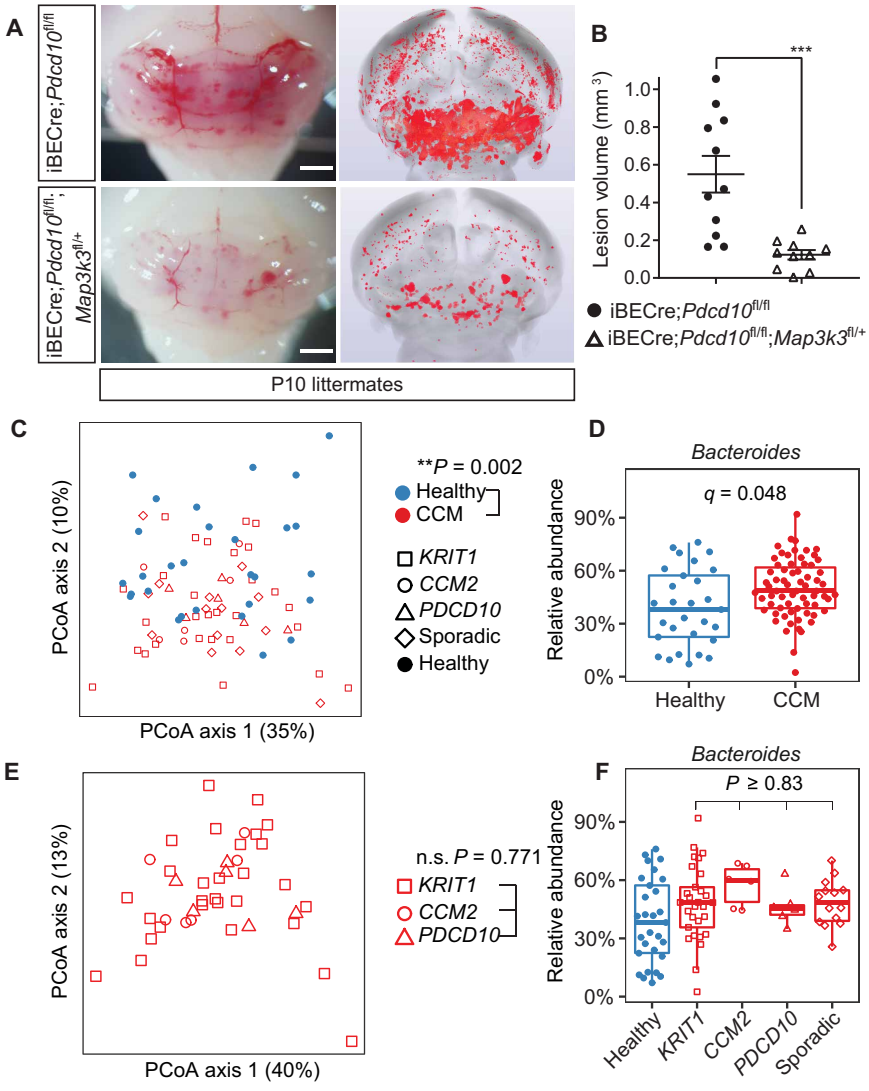

Fig. 1. Comparison of PDCD10, KRIT1, and CCM2 deficiency states in mice and humans. (**A**) CCM lesion burden in iBECre;*Pdcd10*$^{fl/fl}$ and iBECre;*Pdcd10*$^{fl/fl}$ Map3k3$^{fl/+}$ mice at P10, assessed visually (left) and using microCT imaging (right). Scale bars, 1 mm. (**B**) Blinded microCT quantitation of CCM lesion burden in P10 iBECre;*Pdcd10*$^{fl/fl}$ and iBECre;*Pdcd10*$^{fl/fl}$;*Map3k3*$^{fl/+}$ littermates. $n > 10$ animals per genotype and 4 distinct litters. (**C**) Principle coordinates analysis (PCoA) of weighted UniFrac bacterial composition distances between the feces of individuals with familial CCM disease associated with mutations in *KRIT1*, *CCM2*, and *PDCD10*, individuals with sporadic CCM disease, and age/sex-matched healthy controls. *P* value compares bacterial compositions between healthy and CCM disease groups using PERMANOVA. (**D**) Relative abundance boxplots of Gram-negative *Bacteroides* in individuals with CCM disease and healthy controls. Significance (false discovery rate, *q*) determined by linear models of logit-transformed relative abundances with Benjamini-Hochberg correction for multiple comparisons. (**E**) PCoA of weighted UniFrac bacterial composition distances between the feces of only individuals with genotyped mutations in *KRIT1*, *CCM2*, and *PDCD10*. *P* values compare bacterial compositions in all groups using PERMANOVA. (**F**) Relative abundance boxplots of Gram-negative *Bacteroides* comparing genotyped familial *KRIT1*, *CCM2*, or *PDCD10* patients with sporadic cases or healthy volunteers. Significance was determined by pairwise testing of estimated marginal means from a linear model comparing the genetic categories of CCM disease, controlling for age and sex. All associated $P > 0.5$ and not significant (n.s.). Error bars shown as SEM and significance (B) determined by unpaired, two-tailed Student's *t* test. ***$P < 0.001$; n.s., $P > 0.05$.

RESULTS

CCM disease genes are not distinguished by their effects on mouse brain endothelial cell signaling or the human gut microbiome

CCMs arise because of loss of negative regulation of MEKK3 signaling in brain endothelial cells [compartment no. 1 in fig. S1A and (*21*)]. We have recently demonstrated that MEKK3 signaling in brain endothelial cells is stimulated by TLR4 receptors that respond to LPS derived from GNB in the gut microbiome [compartment no. 2 in fig. S1A and (*20*)], predicting that LPS must cross the gut barrier and enter the blood to drive CCM formation (compartment no. 3 in fig. S1A). Clinical studies have revealed that CCM disease associated with mutations in *PDCD10* presents decades earlier than that associated with *KRIT1* or *CCM2* mutations and is associated with larger lesions and greater incidence of symptomatic cerebral hemorrhage (*18*, *19*), an

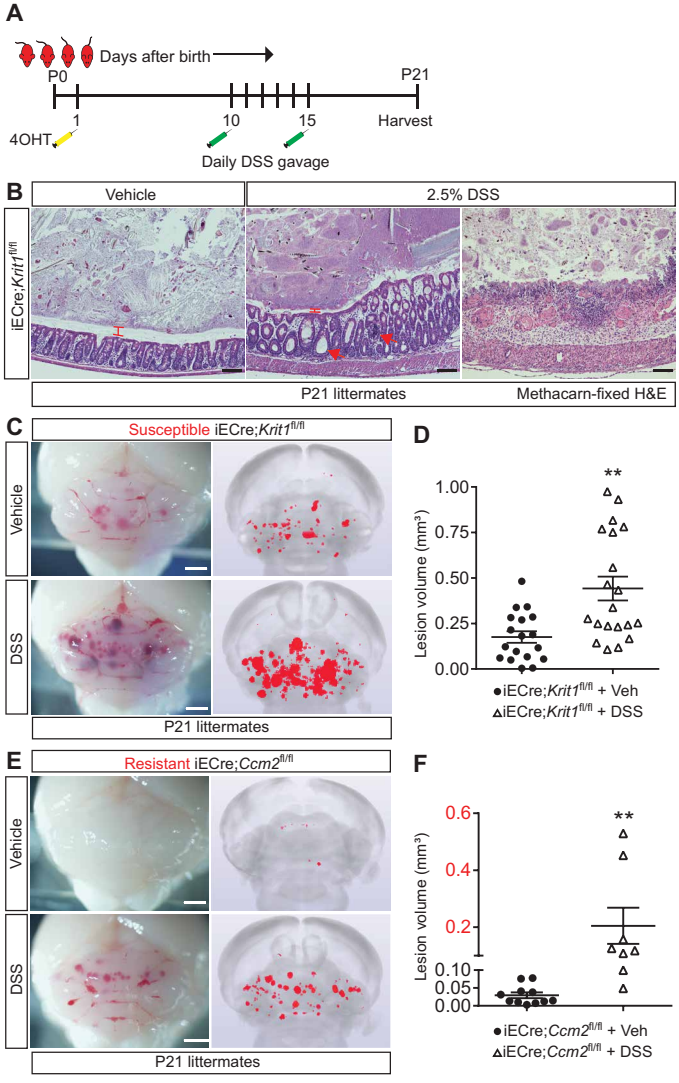

Fig. 2. Effect of dextran sulfate sodium–induced colitis on CCM formation. (**A**) Schematic of the experimental design in which littermates receive an injection of tamoxifen 1 day after birth (P1), daily gavage of dextran sulfate sodium (DSS) or vehicle from P10 to P15, and tissue harvest at P21. 4OHT, 4-hydroxytamoxifen. (**B**) DSS-treated iECre;*Krit1*$^{fl/fl}$ mice exhibit colitis of varying severity associated with thinned mucus layer (red bracket), crypt dilation and abscesses (red arrows), and an inflamed (middle) or entirely eroded (right) epithelium. Scale bars, 100 μm. Results are representative of $n > 3$ animals per treatment group. H&E, hematoxylin and eosin. (**C**) CCM lesion burden in susceptible iECre;*Krit1*$^{fl/fl}$ mice was measured after DSS or vehicle exposure assessed visually (left) and using microCT imaging (right). Scale bars, 1 mm. (**D**) Blinded microCT quantitation of CCM lesion burden in P21 iECre;*Krit1*$^{fl/fl}$ littermates after gavage with vehicle or DSS. $n > 18$ per treatment group and 8 distinct litters. (**E**) CCMs form in resistant iECre;*Ccm2*$^{fl/fl}$ mice after DSS exposure. CCMs were assessed visually (left) and using microCT imaging (right). Scale bars, 1 mm. (**F**) Blinded microCT quantitation of CCM lesion burden in resistant P21 iECre;*Ccm2*$^{fl/fl}$ littermates after gavage with vehicle or DSS. $n \geq 8$ per treatment group and 4 distinct litters. Error bars are shown as SEM, and significance is determined by unpaired, two-tailed Welch's *t* test (D) or unpaired, two-tailed Student's *t* test (F). $^{**}P < 0.01$.

observation not explained by known protein-specific differences in CCM complex function or regulation of the gut microbiome (*13*–*15*, *22*). To determine why *PDCD10* familial disease is particularly severe, we first tested whether the requirement for PDCD10 differs from those of Krev interaction trapped protein 1 (KRIT1) or CCM2 at the levels of brain endothelial MEKK3 signaling or the gut microbiome.

To study CCM formation in vivo, we used an established neonatal mouse model that entails brain endothelial cell–specific deletion of *Pdcd10* using the *Slco1c1(BAC)-CreERT2* (iBECre;*Pdcd10*$^{fl/fl}$, "inducible brain endothelial Cre") 1 day after birth (P1) (fig. S1B) (*23*). iBECre;*Pdcd10*$^{fl/fl}$ mice exhibited CCM lesions with gain of endothelial Kruppel-like factor 4 (KLF4) expression, a downstream hallmark of elevated endothelial MEKK3 signaling that we, and others, have previously identified in *Krit1* and *Ccm2* mouse lesions and human CCMs (fig. S1, C to H) (*13*, *24*, *25*). Similar to analogous genetic rescue experiments using *Krit1* and *Ccm2* animals, haploinsufficiency of MEKK3 in *Pdcd10* littermates resulted in an 80% reduction in lesion volume at P10 assessed visually and through blinded x-ray microcomputed tomography (microCT) imaging of the entire mouse brain (Fig. 1, A and B) (*13*, *26*, *27*). These results indicate that the role of PDCD10 in regulation of endothelial MEKK3 signaling is similar in magnitude to those of KRIT1 and CCM2 and suggest that the basis for more severe PDCD10-associated disease is likely to be an unidentified role for PDCD10 in other cell types or the gut microbiome.

Using the neonatal mouse CCM model, we recently demonstrated that the composition of the gut microbiome plays a vital role in lesion formation, with animals harboring greater numbers of GNB in the colon exhibiting greater CCM lesion formation (fig. S1A, compartment no. 2) (*20*). To test whether patients with *PDCD10*-mediated CCM might exhibit more aggressive disease due to PDCD10-associated changes in the microbiome, we performed 16*S* ribosomal RNA (rRNA) gene sequencing of bacterial DNA extracted from the feces of 75 patients with genotyped CCM with detectable lesions using magnetic resonance imaging and compared these samples to 29 healthy volunteers from multiple clinical sites in the United States (table S1) (*28*). A permutational multivariate analysis of variance (PERMANOVA) test on weighted UniFrac distances revealed a significant ($P = 0.002$) separation of the microbiome communities in patients with CCM disease and those in control individuals (Fig. 1C). Fitting linear models for logit-transformed relative abundances of commonly present bacterial taxa revealed that Gram-negative *Bacteroides* were more abundant in individuals with CCM disease than in controls (Fig. 1D), whereas Gram-positive *Lachnospiraceae* were less abundant (fig. S1I). Individuals with familial *PDCD10* disease did not exhibit microbiomes different from those with familial *KRIT1* or *CCM2* disease, either globally (Fig. 1E) or with respect to changes in Gram-negative *Bacteroides* or Gram-positive *Lachnospiraceae* species (Fig. 1F and fig. S1J). Although conclusions drawn from these data are limited by the relatively small sample size and biased toward symptomatic CCM disease, they support the concept that environmental factors dominate over host genetics to alter gut microbial ecology (*29*). Together, our mouse genetic and human microbiome studies suggest that the basis for a more aggressive clinical course in familial *PDCD10* disease is neither a unique signaling role in brain endothelial cells nor a specific effect on the gut microbiome and therefore might reflect a previously unrecognized role for PDCD10 in the intervening gut barrier.

Chemical disruption of the gut barrier accelerates CCM formation in mice

To test whether disruption of the gut barrier worsens CCM disease, we combined the dextran sulfate sodium (DSS) colitis and neonatal

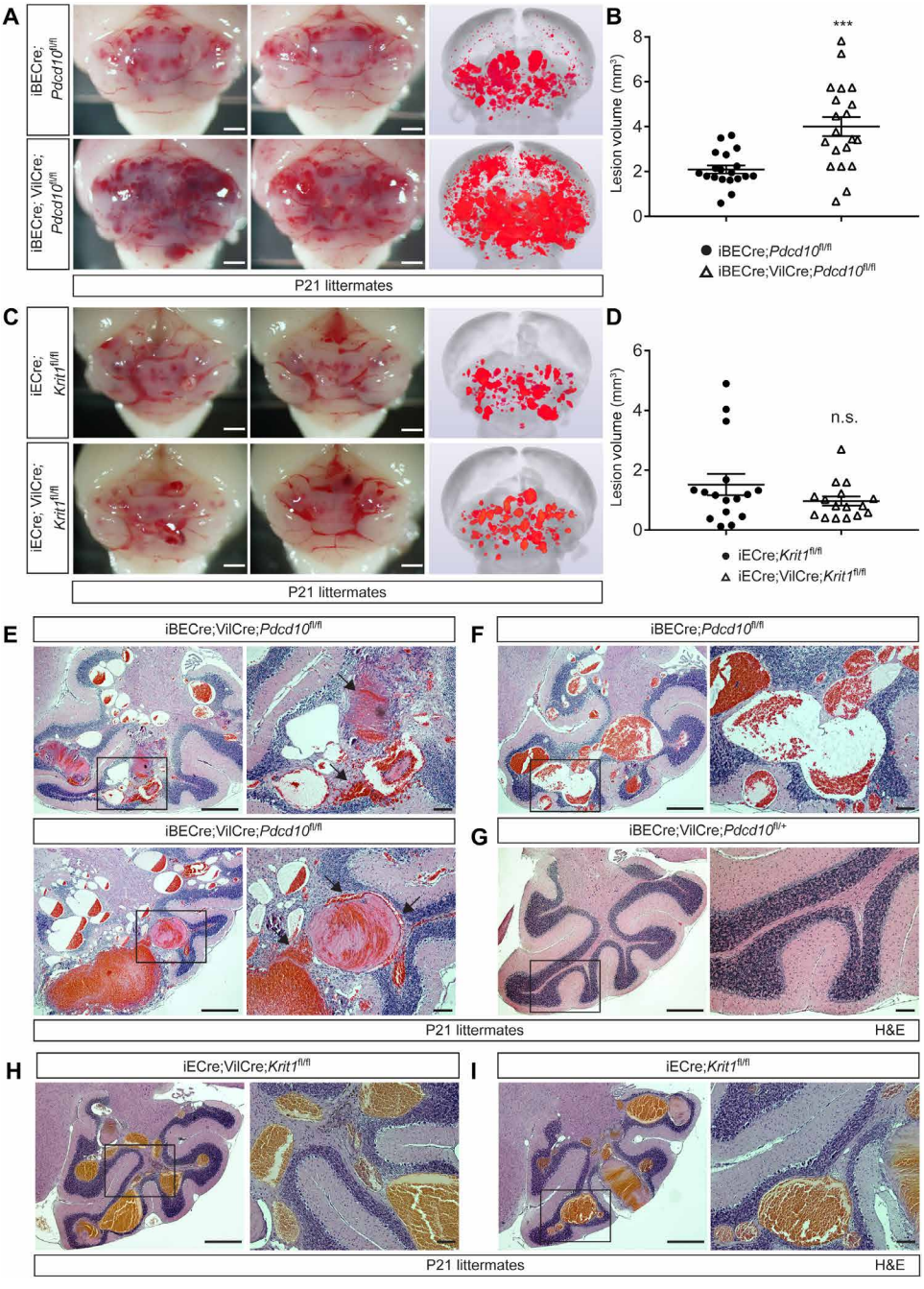

Fig. 3. Effect of brain endothelial and gut epithelial loss of PDCD10 or KRIT1 on CCM formation. (**A**) CCM formation in iBECre;*Pdcd10*$^{fl/fl}$ and iBECre;VilCre;*Pdcd10*$^{fl/fl}$ littermates assessed visually (left and middle) and using microCT imaging (right). Scale bars, 1 mm. (**B**) Blinded microCT quantitation of CCM lesion burden in P21 iBECre;*Pdcd10*$^{fl/fl}$ and iBECre;VilCre;*Pdcd10*$^{fl/fl}$ littermates. $n \geq 19$ animals per genotype and 10 distinct litters. (**C**) CCM formation in iECre;*Krit1*$^{fl/fl}$ and iECre;VilCre;*Krit1*$^{fl/fl}$ littermates was assessed visually (left and middle) and using microCT imaging (right). Scale bars, 1 mm. (**D**) Blinded microCT quantitation of CCM lesion burden in P21 iECre;*Krit1*$^{fl/fl}$ and iECre;VilCre;*Krit1*$^{fl/fl}$ littermates. $n \geq 16$ animals per genotype and 7 distinct litters. (**E** to **G**) H&E staining of hindbrain sections from P21 iBECre;VilCre;*Pdcd10*$^{fl/fl}$, iBECre;*Pdcd10*$^{fl/fl}$, and iBECre;VilCre;*Pdcd10*$^{fl/+}$ littermates. Arrows indicate extravascular hemorrhage that was observed in iBECre;VilCre;*Pdcd10*$^{fl/fl}$ animals. Boxes in left images denote area of magnified image on the right. Scale bars, 500 μm (left images) and 100 μm (right images). (**H** and **I**) H&E staining of hindbrain sections from P21 iECre;Krit1$^{fl/fl}$ and iECre;VilCre;Krit1$^{fl/fl}$ littermates. Boxes in left images denote area of magnified image on the right. Scale bars, 500 μm (left images) and 100 μm (right images). Results are representative of $n \geq 3$ animals per genotype and 4 distinct litters. Error bars are shown as SEM, and significance is determined by unpaired, two-tailed Welch's *t* test. ***$P < 0.001$; n.s., $P > 0.05$.

CCM mouse models. As previously described (*13*), to initiate the neonatal CCM model, we induced endothelial cell–specific deletion of *Krit1* at P1 using the *Cdh5(PAC)-CreERT2* (iECre;*Krit1*$^{fl/fl}$, "inducible endothelial Cre"). Starting at P10, 2.5% DSS was orally administered once daily for 5 days, resulting in varying degrees of colitis ranging from epithelial thickening and crypt abscesses to complete erosion of the colonic epithelium at P21, with colitis observed in five animals treated with DSS and no colitis in four controls ($P < 0.05$; Fig. 2, A and B). About 50% of neonatal animals administered DSS did not survive to P21 (likely a result of DSS effects and lethality associated with gavaging neonatal mice), but survivors (20 of 45 total animals) exhibited an approximate twofold increase in CCM volume compared to littermate, vehicle-treated animals (Fig. 2, C and D).

We previously characterized distinct *Krit1* and *Ccm2* mouse colonies that are respectively resistant and susceptible to CCM formation because of qualitative differences in the gut microbiome (*20*). Susceptible, vehicle-treated iECre;*Krit1*$^{fl/fl}$ animals spontaneously developed appreciable lesion volume (Fig. 2, C and D), whereas resistant, vehicle-treated iECre;*Ccm2*$^{fl/fl}$ animals exhibited barely detectable lesions (Fig. 2, E and F). Analogous to the *Krit1* experiments performed in susceptible animals, resistant, DSS-treated iECre;*Ccm2*$^{fl/fl}$ animals exhibited a 10-fold increase in lesion volume (Fig. 2, E and F). These results demonstrate that broad disruption of the colonic epithelium exacerbates CCM disease in a manner independent of genotype or baseline microbiome.

Gut epithelial loss of PDCD10 but not KRIT1 accelerates CCM lesion formation

The exacerbation of CCM formation by DSS treatment identified the gut barrier as a potentially rate-limiting mechanism of disease pathogenesis. Although the gut barrier is a complex, multicellular system, its primary component is the gut epithelium. Analysis of single-cell gene expression in intestinal epithelial cells (IECs) revealed broad transcription of *Krit1*, *Ccm2*, and *Pdcd10* across cell types (fig. S2). We therefore hypothesized that PDCD10 might play a role in gut barrier integrity distinct from that of KRIT1 and

CCM2. To study the role of IEC PDCD10 in the context of CCM disease, we compared CCM formation in animals with both inducible brain endothelial cell deletion (iBECre) at P1 and constitutive IEC deletion (Villin1-Cre, "VilCre") of *Pdcd10* (iBECre;VilCre;*Pdcd10*$^{fl/fl}$), to littermates with only inducible brain endothelial cell deletion of *Pdcd10* (iBECre;*Pdcd10*$^{fl/fl}$). Loss of IEC *Pdcd10* resulted in a two-fold increase in lesion burden by P21 (Fig. 3, A and B). To determine whether PDCD10 plays a specific role in IECs during CCM formation relative to the other CCM genes, we performed the analogous *Krit1* experiment. Loss of IEC *Krit1* had no effect on lesion formation (Fig. 3, C and D).

A notable clinical aspect of familial *PDCD10* disease is the high rate of cerebral hemorrhage compared with familial *KRIT1* or *CCM2* disease (*19*). Histologic examination of iBECre;VilCre;*Pdcd10*$^{fl/fl}$ mouse brains at P21 revealed both large CCM lesions in the white matter of the cerebellum and numerous sites of perilesional hemorrhage (Fig. 3E and fig. S3A). Although large, multicavernous lesions were also observed in iBECre;*Pdcd10*$^{fl/fl}$ brains, after deletion of *Pdcd10* solely in the brain endothelium (Fig. 3F and fig. S3A), no perilesional hemorrhage was observed, consistent with prior studies of the neonatal CCM model (*30*). Hemorrhage was not observed in either animals with loss of only a single *Pdcd10* allele in the brain endothelium and IECs, animals with complete loss of *Pdcd10* only in IECs (Fig. 3G and fig. S3, B to E), or in either iECre;VilCre;*Krit1*$^{fl/fl}$ or iECre;*Krit1*$^{fl/fl}$ mouse brains at P21 (Fig. 3, H and I, and fig. S3A). These findings identify a role for PDCD10 in the gut epithelium during CCM formation in mice distinct from that of KRIT1.

Loss of gut epithelial PDCD10 but not KRIT1, CCM2, or MEKK3 results in loss of the colonic mucus layer

Because most GNB and GNB-derived LPS reside in the colon, to understand the role of PDCD10 in IECs during CCM formation, we analyzed the colons of the same iBECre;*Pdcd10*$^{fl/fl}$ and iBECre;VilCre;*Pdcd10*$^{fl/fl}$ animals shown in Fig. 3 (Fig. 4A). Because individuals with familial *PDCD10* disease are germline heterozygous, we also analyzed colons from littermate iBECre;VilCre;*Pdcd10*$^{fl/+}$ animals (Fig. 4A, middle). A major component of the colonic gut barrier is the mucus layer, produced by goblet cells, that physically separates gut bacteria from the gut epithelium (*31*), and an initial event in DSS-associated colitis is disruption of the mucus barrier (*32*). Analysis of the colonic mucus barrier using methacarn-fixed samples [fig. S4 and (*31*, *33*)] revealed a significant ($P < 0.0001$) reduction of the mucus layer after homozygous or heterozygous loss of IEC *Pdcd10* at P21 (Fig. 4, A and C). In contrast, loss of IEC *Krit1, Ccm2*, or *Map3k3* had no effect on mucus layer dimensions at P21 (Fig. 4, B and D, and figs. S5 and S6). In addition, loss of IEC PDCD10 was associated with markedly swollen goblet cells (Fig. 4A and fig. S7A) but no change in the expression of *Muc2* mRNA or Mucin-2 (MUC2) protein (fig. S7, C to F), whereas loss of IEC *Krit1* was not associated with any change in goblet cell vesicle size (Fig. 4B and fig. S7B).

VilCre;*Pdcd10*$^{fl/+}$ and VilCre;*Pdcd10*$^{fl/fl}$ animals exhibited increased concentration of fecal lipocalin-2 (LCN2 aka NGAL), a secreted inflammatory response protein that has been shown to be a sensitive and dynamic marker of colitis (Fig. 4E) (*34*) that was not observed after IEC loss of *Krit1*, *Ccm2*, or *Map3k3* (Fig. 4F and figs. S5 and S6). Consistent with the rise in fecal LCN2, P21 iBECre;VilCre;*Pdcd10*$^{fl/+}$ and iBECre;VilCre;*Pdcd10*$^{fl/fl}$ colons exhibited crypt dilation, an early sign of inflammation (Fig. 4A and fig. S7G), and crypt abscesses marked by lymphocyte antigen 6 complex, locus G (Ly6G)–positive neutrophils (Fig. 4, G and I). In contrast, P21 iECre;VilCre;*Krit1*$^{fl/fl}$ animals exhibited normal colonic crypts without crypt abscesses (Fig. 4, B, H, and J, and fig. S7H).

Our prior studies have demonstrated that the amount of circulating LPS determines CCM formation in mouse models, suggesting that loss of gut barrier function associated with IEC PDCD10 deficiency might augment CCM formation by permitting more translocation of GNB-derived LPS from the gut lumen to the circulating blood (*20*). Consistent with such a mechanism, loss of IEC PDCD10 resulted in elevated TLR4 agonist activity in circulating blood from P21 animals (Fig. 4K). In contrast, loss of IEC KRIT1 had no effect on TLR4 agonist activity in circulating blood from P21 animals (Fig. 4L). An increase in blood TLR4 activation was not detected in animals with heterozygous loss of IEC *Pdcd10* (iBECre;VilCre;*Pdcd10*$^{fl/+}$), most likely because of a low basal rate of leak/translocation and the limited sensitivity of measuring circulating LPS at a single time point compared with growth of CCM lesions over 21 days (Fig. 4K).

Genetic loss of colonic mucus accelerates CCM formation in mice

The studies described above suggested that a primary mechanism by which PDCD10 deficiency in IECs might accelerate CCM formation is through loss of the mucus layer that prevents GNB from reaching the gut wall and translocating to the blood (*31*–*33*, *35*–*37*). To directly test the role of the mucus layer in CCM formation, we examined the effect of loss of MUC2, a glycoprotein secreted by goblet cells that is the primary constituent of the colonic mucosal barrier (*33*, *37*), on lesion formation after *Pdcd10* gene deletion in brain endothelial cells at P1. Loss of one or two *Muc2* alleles conferred a dose-dependent decrease in both the mucus layer and CCM lesion volume of P21 animals similar to those observed after loss of one or two *Pdcd10* alleles in IECs (Fig. 5, A to D).

The CCM proteins, particularly KRIT1, have been implicated in the maintenance of endothelial junctions, and epithelial junction integrity is another component of the gut barrier underlying colonic mucus (*38*, *39*). Loss of gut epithelial PDCD10 resulted in decreased E-cadherin (CDH1) but increased epithelial cell adhesion molecule (EpCAM) junction continuity and no changes in F-actin or zonula occludens-1 (ZO-1), whereas loss of gut epithelial KRIT1 did not affect junctions (figs. S8, A to D; S9, A to D; and S10). *Muc2*-null colons exhibited decreased E-cadherin and EpCAM junction continuity, but *Muc2* heterozygous colonic epithelial junctions were unchanged (figs. S8, E and F, and S9, E and F). Thus, *Muc2* heterozygosity worsens CCM burden in the setting of a decreased colonic mucus barrier but unchanged epithelial junctions. Overall, these findings suggest that a primary mechanism by which *Pdcd10* prevents CCM formation in IECs is through its role in maintaining the colonic mucus layer.

The gut barrier can regulate CCM formation independent of the gut microbiome

In addition to providing a protective layer for the intestinal epithelium, the abundant glycoprotein MUC2 serves as a food source for luminal bacteria and affects microbial ecology (*40*). Moreover, MUC2 secretion by goblet cells is bacterial-ligand dependent and affected by qualitative differences in the gut microbiome (*36*, *41*). Thus, changes in mucus expression could affect CCM formation through changes in the gut microbiome and the gut barrier. To address the relationship between the gut barrier and the gut microbiome,

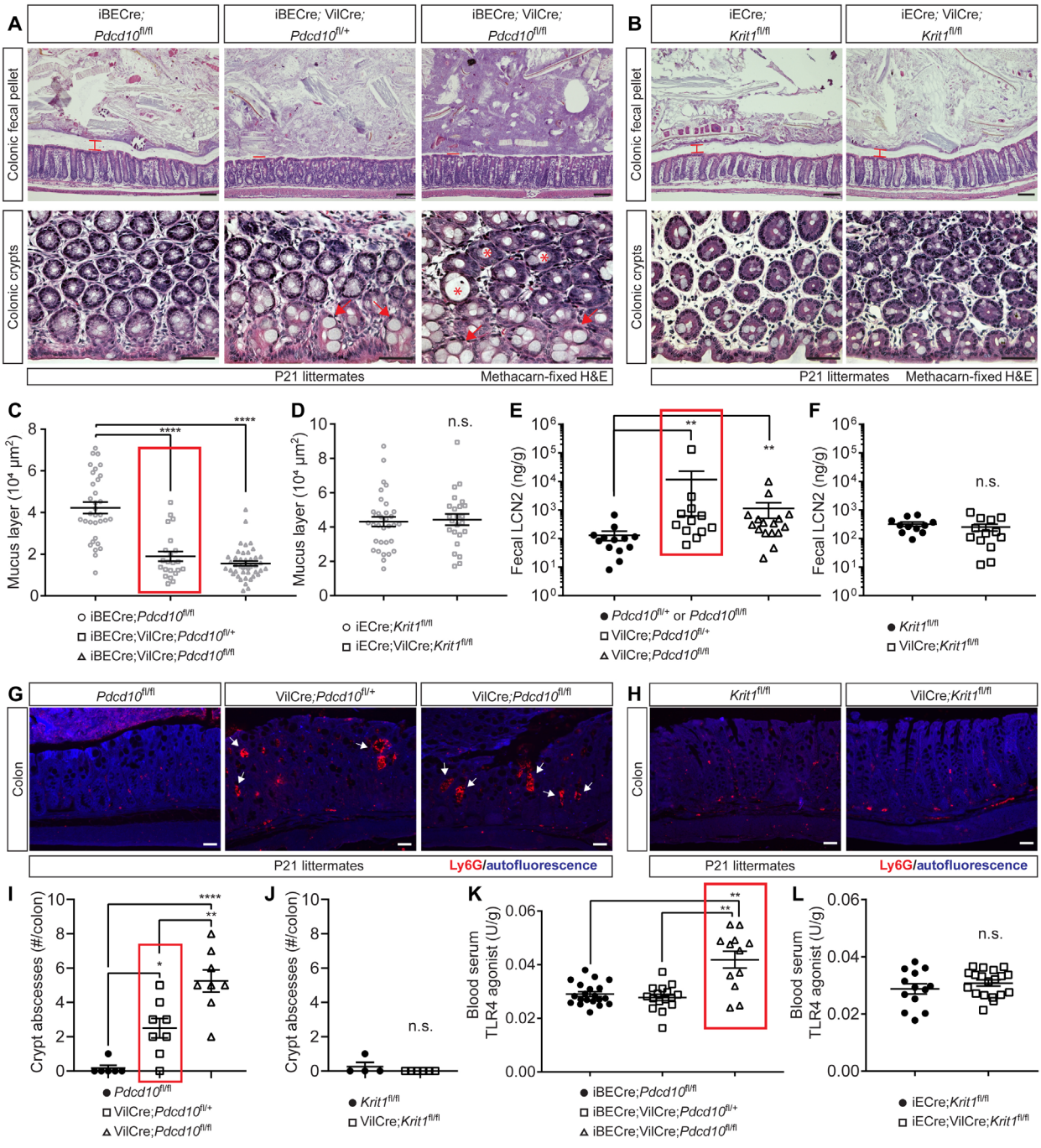

Fig. 4. Gut barrier and blood TLR4 ligand after gut epithelial loss of PDCD10 or KRIT1. (**A** and **B**) H&E histology of methacarn-fixed colons from iBECre;*Pdcd10*$^{fl/fl}$, iBECre;VilCre;*Pdcd10*$^{fl/+}$, and iBECre;VilCre;*Pdcd10*$^{fl/fl}$ animals (A) or iECre;*Krit1*$^{fl/fl}$ and iECre;VilCre;*Krit1*$^{fl/fl}$ animals (B) at P21. Low-magnification images of the colonic fecal pellet (top) and higher-magnification images of the colonic crypts (bottom). The brains of these animals with CCM lesions are shown in Fig. 3. Brackets denote the thickness of the mucus layer. Arrows indicate goblet cells. Asterisks highlight colonic crypts. Scale bars, 100 μm (top) and 50 μm (bottom). Results are representative of $n \geq 16$ animals per genotype and at least 7 distinct litters. (**C** and **D**) Quantitation of colonic mucus layer from the indicated H&E-stained, methacarn-fixed, tissue sections in (A) and (B). Each point represents measurements around one fecal pellet, $n \geq 16$ animals per genotype and at least 7 distinct litters. (**E**) Fecal lipocalin-2 (LCN2) concentration measured by enzyme-linked immunosorbent assay (ELISA) in VilCre;*Pdcd10*$^{fl/fl}$, VilCre;*Pdcd10*$^{fl/+}$, or littermate controls (*Pdcd10*$^{fl/+ \text{ or } fl/fl}$). $n \geq 12$ animals per genotype from 4 distinct litters. (**F**) Fecal LCN2 concentration measured by ELISA in VilCre;*Krit1*$^{fl/fl}$ and littermate *Krit1*$^{fl/fl}$ animals. $n \geq 11$ animals per genotype and 3 distinct litters. (**G** and **H**) Immunostaining for the neutrophil marker Ly6G is shown for P21 colons from *Pdcd10*$^{fl/fl}$, VilCre;*Pdcd10*$^{fl/+}$, and VilCre;*Pdcd10*$^{fl/fl}$ littermates as well as *Krit1*$^{fl/fl}$ and VilCre;*Krit1*$^{fl/fl}$ littermates. Scale bars, 50 μm. (**I** and **J**) Quantification of Ly6G-positive crypt abscesses per colonic section analyzed. Each point represents a distinct animal. Results are representative of $n \geq 4$ animals per genotype and at least 3 distinct litters. (**K** and **L**) TLR4 agonist activity detected in the blood of VilCre;*Pdcd10*$^{fl/fl}$ animals and VilCre;*Krit1*$^{fl/fl}$ animals. $n \geq 13$ animals per genotype and at least 7 distinct litters. Error bars are shown as SEM, and significance is determined by Kruskal-Wallis one-way ANOVA with Dunn's correction for multiple comparisons (C, E, and I) or unpaired, two-tailed Student's *t* test (D, F, and J). ****$P < 0.0001$, **$P < 0.01$; n.s., $P > 0.05$.

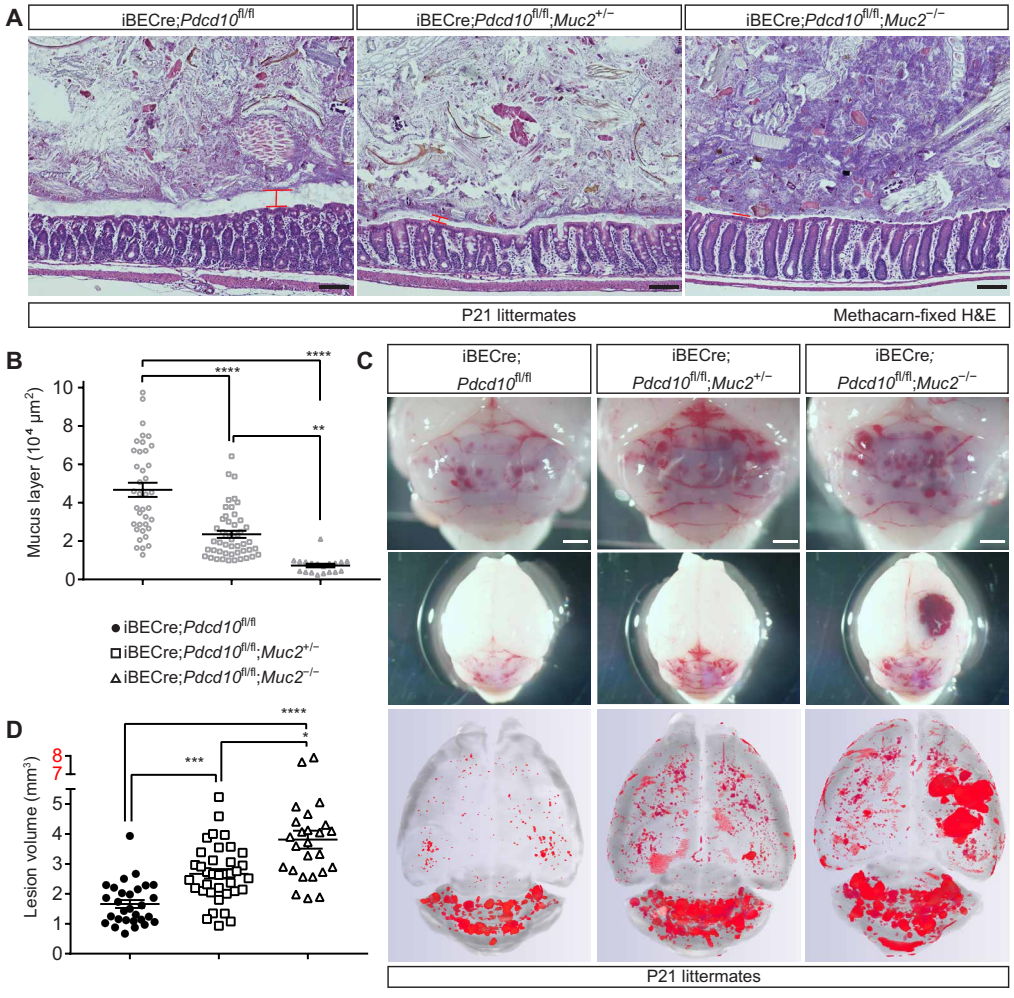

Fig. 5. Relationship of the colonic mucus barrier and CCM formation. (**A**) H&E staining of methacarn-fixed colon samples from iBECre;*Pdcd10*$^{fl/fl}$, iBECre;*Pdcd10*$^{fl/fl}$;*Muc2*$^{+/-}$, and iBECre;*Pdcd10*$^{fl/fl}$;*Muc2*$^{-/-}$ animals. The mucus barrier is indicated with brackets. Scale bars, 100 μm. (**B**) Quantitation of the area of the mucus layers shown in (A). Each point represents measurement around one fecal pellet. $n \geq 10$ animals per genotype and 9 distinct litters. (**C**) CCM formation in representative P21 iBECre;*Pdcd10*$^{fl/fl}$, iBECre;*Pdcd10*$^{fl/fl}$;*Muc2*$^{+/-}$, and iBECre;*Pdcd10*$^{fl/fl}$;*Muc2*$^{-/-}$ animals is shown visually in the hindbrain (top), hindbrain and forebrain (middle), and with microCT imaging (bottom). Scale bars, 1 mm. (**D**) Blinded microCT quantification of CCM lesion volumes in P21 iBECre;*Pdcd10*$^{fl/fl}$, iBECre;*Pdcd10*$^{fl/fl}$;*Muc2*$^{+/-}$, and iBECre;*Pdcd10*$^{fl/fl}$;*Muc2*$^{-/-}$ littermates. $n \geq 25$ animals per genotype and 17 distinct litters. Error bars are shown as SEM, and significance is determined by Kruskal-Wallis one-way ANOVA with Dunn's correction for multiple comparisons (B and D). ****$P < 0.0001$, ***$P < 0.001$, **$P < 0.01$, *$P < 0.05$.

we next performed 16*S* rRNA gene sequencing of bacterial DNA extracted from the feces of mice with genetic loss of epithelial *Pdcd10*, *Krit1*, or *Muc2*. Because cage and litter effects are a confounding factor in gut microbiome studies (*42*), we collected fecal pellets from P21 animals before weaning when the entire litter remained cohoused (Fig. 6A), and all analyses were performed considering individual cage effects (fig. S11). A PERMANOVA test of unweighted UniFrac distances revealed a separation of bacterial microbiome communities from VilCre;*Pdcd10*$^{fl/fl}$ mice compared with either VilCre;*Pdcd10*$^{fl/+}$ or *Pdcd10*$^{fl/fl}$ littermates (Fig. 6B and figs. S11A and S12A). A similar separation was observed when iBECre;VilCre;*Pdcd10*$^{fl/fl}$ animals were compared with iBECre;VilCre;*Pdcd10*$^{fl/+}$ or iBECre;*Pdcd10*$^{fl/fl}$ littermates (Fig. 6C and figs. S11B and S12B). A significant ($P < 0.001$) separation of bacterial microbiome communities was also observed between iBECre;*Pdcd10*$^{fl/fl}$;*Muc2*$^{-/-}$ when compared to either iBECre;*Pdcd10*$^{fl/fl}$;*Muc2*$^{+/-}$ or iBECre;*Pdcd10*$^{fl/fl}$;*Muc2*$^{+/+}$ littermates (Fig. 6D and figs. S11C and S12C). In contrast, no significant ($P = 0.311$) separation of bacterial microbiome communities was observed between *Krit1*$^{fl/fl}$ and VilCre;*Krit1*$^{fl/fl}$ animals (Fig. 6E and figs. S11D and S12D). Fitting generalized, linear mixed-effects models for logit-transformed relative abundances of commonly present bacterial taxa identified almost identical shifts for VilCre;*Pdcd10*$^{fl/fl}$, iBECre;VilCre;*Pdcd10*$^{fl/fl}$, and iBECre;*Pdcd10*$^{fl/fl}$;*Muc2*$^{-/-}$ animals, including a significant ($q \leq 0.05$) increase in *Bacteroides* and *Rikenellaceae* species and decrease in *s24-7*, *Prevotellaceae*, and *Alloprevotella* species (Fig. 6F and fig. S13). The observation that loss of gut epithelial *Pdcd10* conferred biome changes indistinguishable from those associated with loss of *Muc2* provides additional evidence that a major effect of IEC PDCD10 loss is disruption of the colonic mucosal barrier composed of MUC2. Analysis of heterozygous VilCre;*Pdcd10*$^{fl/+}$, iBECre;VilCre;*Pdcd10*$^{fl/+}$, and iBECre;*Pdcd10*$^{fl/fl}$;*Muc2*$^{+/-}$ animals revealed no significant ($q > 0.05$) changes in the gut microbiome (Fig. 6G), although iBECre;*Pdcd10*$^{fl/fl}$;*Muc2*$^{+/-}$ animals exhibited increased CCM formation. These findings support the conclusion that changes in gut barrier may influence CCM formation independent of changes in the gut microbiome.

The dietary emulsifier P80 degrades colonic mucus and accelerates CCM formation in mice

The studies of DSS exposure and IEC loss of PDCD10 and MUC2 described above suggested that dietary agents that reduce the colonic mucosal barrier may accelerate CCM disease. A recent study reported that dietary emulsifiers, such as those commonly found in processed foods, promote colitis by degrading the colonic mucosal barrier (*43*). To test whether ingestion of a common dietary emulsifier might drive CCM formation through changes in the gut barrier, we first exposed *Pdcd10*$^{+/-}$ animals to oral 1% P80 emulsifier for 2 weeks and assessed

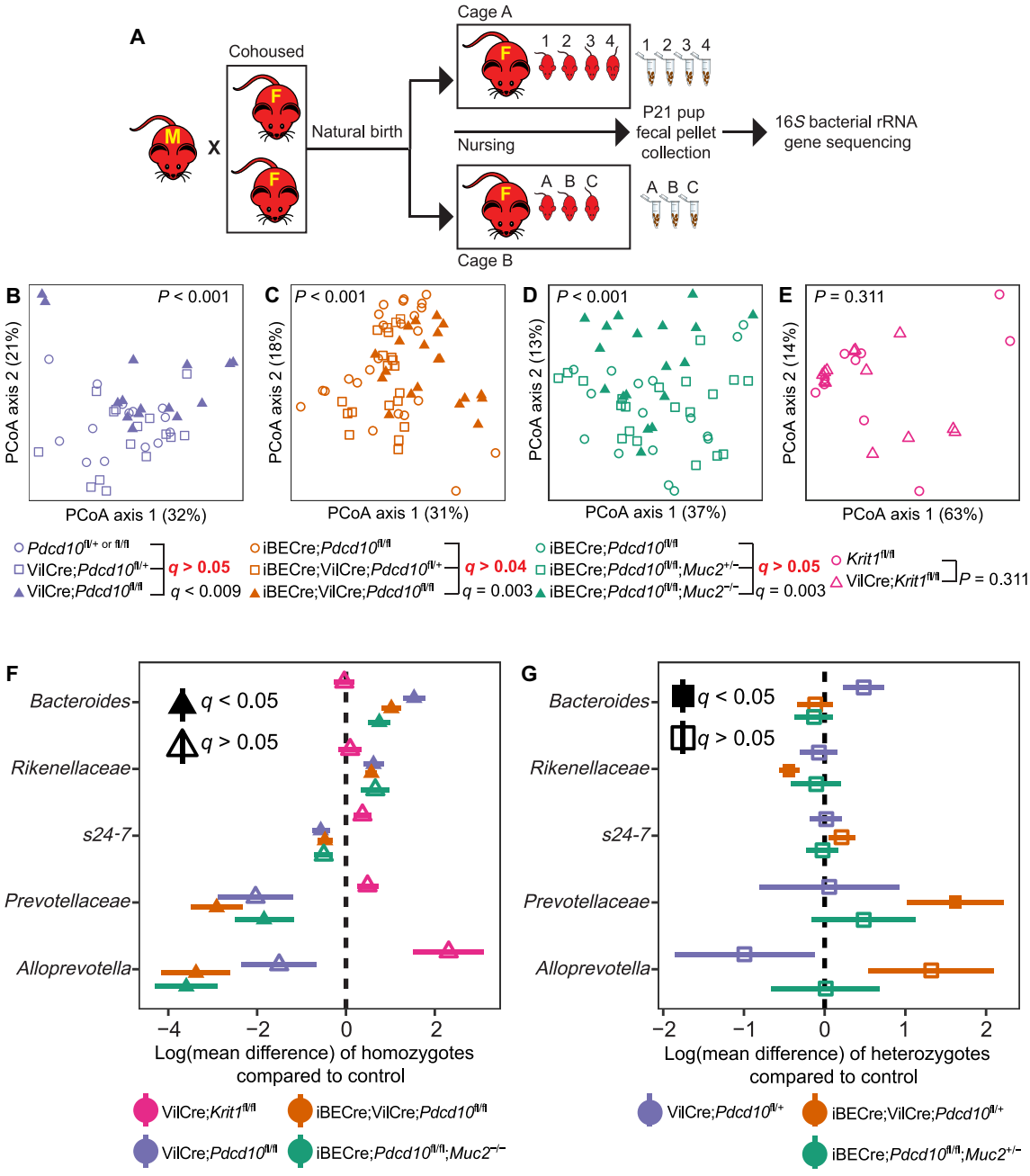

Fig. 6. Analysis of the gut microbiome after loss of gut epithelial PDCD10 or MUC2. (**A**) Experimental design in which females were mated, individually housed before natural delivery of pups, and fecal pellets collected from each pup at P21 before weaning for 16*S* rRNA bacterial gene sequencing. (**B** to **E**) PCoA of weighted UniFrac bacterial composition distances from the feces of the indicated animals. Each box shows analysis of littermate animals while accounting for caging differences. *P* values compare bacterial compositions in the indicated groups using PERMANOVA also considering individual cage differences and corrected for multiple comparisons using the Bonferroni method. (B to D) $n \geq 10$ animals per genotype and at least 4 distinct cages/litters. Overall *P* values comparing homozygous animals to wild-type or heterozygous controls are shown in plot, as well as the pairwise comparisons (*q* values) in legend. (**F**) Mean difference of logit-transformed relative abundance of the indicated bacteria taxa estimated with linear mixed-effects models in VilCre;*Krit1*$^{fl/fl}$, VilCre;*Pdcd10*$^{fl/fl}$, iBECre;VilCre;*Pdcd10*$^{fl/fl}$, and iBECre;*Pdcd10*$^{fl/fl}$;*Muc2*$^{-/-}$ animals compared to their respective VilCre-negative or *Muc2*$^{+/+}$ littermate controls. (**G**) Mean difference of logit-transformed relative abundance of the indicated bacteria taxa estimated with linear mixed-effects models in VilCre;*Pdcd10*$^{fl/+}$, iBECre;VilCre;*Pdcd10*$^{fl/+}$, and iBECre;*Pdcd10*$^{fl/fl}$;*Muc2*$^{+/-}$ animals compared to their respective VilCre-negative or *Muc2*$^{+/+}$ littermate controls. Significance (false discovery rate, *q*) determined by linear mixed-effects models with Benjamini-Hochberg correction for multiple comparisons.

the thickness of the colonic mucus layer. P80 emulsifier exposure resulted in a 50% reduction in the mucus layer (Fig. 7, A and B). 16*S* rRNA gene sequencing of bacterial DNA extracted from the feces of *Pdcd10*$^{+/-}$ mice treated with P80 or vehicle alone revealed that chronic emulsifier exposure did not result in a significant ($P > 0.05$) separation of bacterial microbiome communities when accounting for cage effects (Fig. 7, C and D, and fig. S14). We next assessed whether chronic exposure to DSS could affect CCM formation. Although

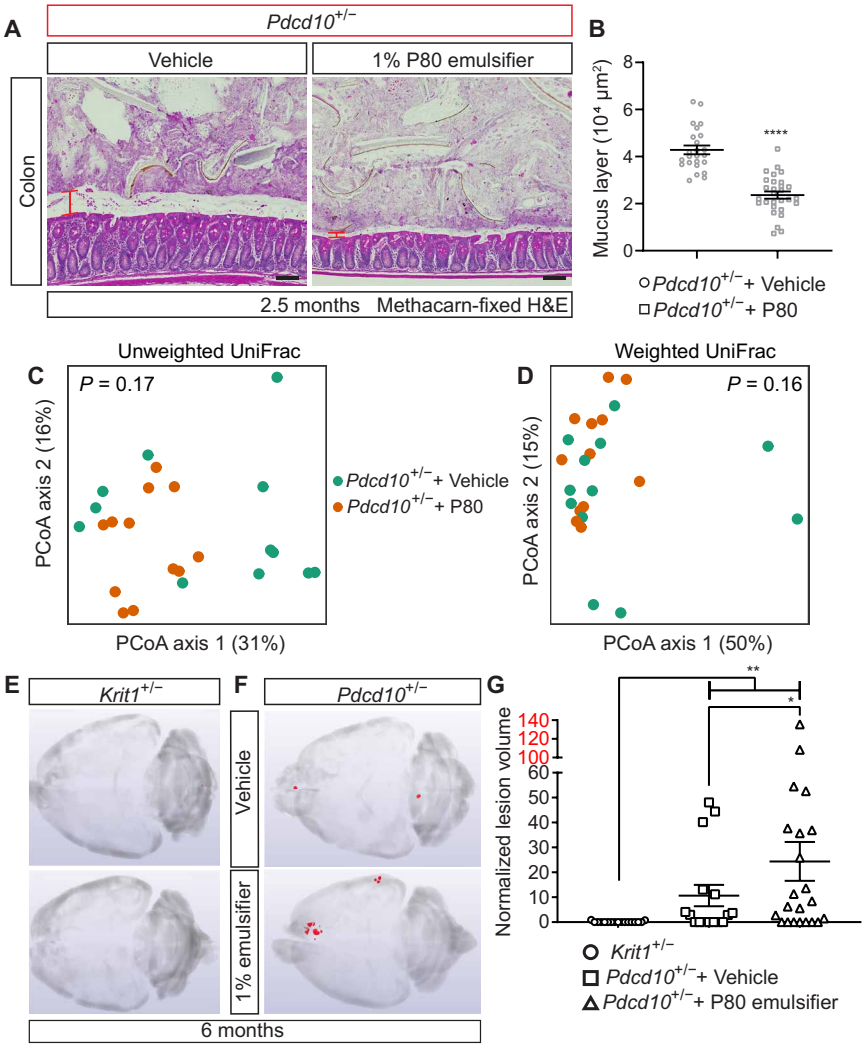

Fig. 7. Effects of chronic P80 dietary emulsifier intake on the colonic mucosal barrier and CCM formation. (**A**) H&E staining of methacarn-fixed colon samples from vehicle and *Pdcd10*$^{+/-}$ animals administered 1% P80 in drinking water for 2 weeks. The mucus barrier is indicated with brackets. Scale bars, 100 µm. (**B**) Quantitation of the area of the mucus layers shown in (A). Each point represents measurement around one fecal pellet. $n = 7$ animals per genotype. (**C** and **D**) PCoA of unweighted and weighted UniFrac bacterial composition distances from the feces of the indicated animals administered 1% P80 for 4 months is shown. *P* values compare bacterial compositions in the indicated groups using PERMANOVA also considering individual cage differences and corrected for multiple comparisons using the Bonferroni method. $n = 12$ animals per genotype and 5 distinct cages per treatment. (**E** to **G**) Spontaneous CCM formation was analyzed using microCT imaging (E and F) and lesion volume measurement normalized to total brain volume (G) in animals of the indicated genotypes administered 1% P80 for 4 months. $n \geq 16$ animals per treatment group. Error bars are shown as SEM, and significance is determined by Kruskal-Wallis one-way ANOVA with Dunn's correction for multiple comparisons (B and D) or Mann-Whitney nonparametric *U* test (G). ****$P < 0.0001$, **$P < 0.01$, *$P < 0.05$.

aged *Krit1*$^{+/-}$ animals exhibited no detectable lesion formation after 6 months (Fig. 7, E and G), aged *Pdcd10*$^{+/-}$ animals exhibited a low but significant ($P < 0.01$) rate of spontaneous lesion formation (Fig. 7, F and G). Chronic treatment of *Pdcd10*$^{+/-}$ animals with 1% P80 significantly ($P < 0.05$) increased lesion formation (Fig. 7, F and G). These studies suggest that emulsifiers commonly found in preserved or processed foods may exacerbate CCM formation through effects on the gut mucosal barrier that are independent of the gut microbiome.

Dexamethasone potently inhibits CCM formation through dual effects on brain endothelial cells and gut epithelial cells

The studies described above and our prior studies (*20*) identify a gut-brain CCM disease axis in which PDCD10 functions in both IECs and brain endothelial cells to control the movement of LPS from the gut lumen into the blood and the response to blood-borne LPS in the brain. This model predicts that therapies able to simultaneously increase gut barrier function by IECs and reduce TLR4-MEKK3-KLF2/4 signaling by brain endothelial cells might potently inhibit CCM formation. Glucocorticoids confer pleiotropic cell and organ effects that are primarily mediated by gene expression changes downstream of glucocorticoid receptor (GR) NR3C1 signaling (*44*). Loss of GR function confers increased responses to LPS in endothelial cells (*45*, *46*), whereas the glucocorticoid dexamethasone increases MUC2 expression by IECs (*47*), suggesting that dexamethasone, a highly selective GR agonist (*48*), might act at both ends of the CCM gut-brain disease axis to prevent lesion formation.

A single dose of dexamethasone administered at P5 entirely blocked CCM formation in both iECre;*Krit1*$^{fl/fl}$ and iECre;*Pdcd10*$^{fl/fl}$ neonates (Fig. 8, A to C, and fig. S15, A to E). The effect of dexamethasone blocked lesion formation using a single dose as low as 0.4 mg/kg (Fig. 8A), less than that commonly administered for asthma exacerbations in human patients. Analysis of brain endothelial gene expression revealed marked reductions in the mRNA transcripts of *Map3k3* (*Mekk3*) as well as the downstream MEKK3 targets *Klf2* and *Klf4* and the upstream MEKK3 activators *Tlr4* and *Cd14* after dexamethasone administration (Fig. 8D).

To test whether rescue was mediated by changes in brain endothelial cells, the effect of dexamethasone was examined in iECre;*Krit1*$^{fl/fl}$;*Nr3c1*$^{fl/fl}$ animals in which endothelial loss of KRIT1 is accompanied by endothelial loss of GR. Dexamethasone treatment continued to potently prevent lesion formation in iECre;*Krit1*$^{fl/fl}$;*Nr3c1*$^{fl/fl}$ animals (Fig. 8, E and F), indicating that the effect of dexamethasone was not merely due to effects in brain endothelial cells. Analysis of the intestine of dexamethasone-treated animals revealed marked colonic dilatation (fig. S15E) that was accompanied by a large increase in goblet cell activity and MUC2 production (Fig. 8, G and H, and fig. S15, F to H). The increase in mucus production stimulated by dexamethasone was ablated in VilCre;*Nr3c1*$^{fl/fl}$ animals (fig. S15, I and J), indicating that it is mediated by stimulation of IEC GR. To test whether dexamethasone rescue of CCM formation is mediated primarily by effects on IEC mucus production, we examined rescue in mice lacking MUC2. Dexamethasone potently prevented lesion formation in iBECre;*Pdcd10*$^{fl/fl}$;*Muc2*$^{-/-}$ animals (Fig. 8, I to K), indicating that rescue was also not merely due to effects on IECs. To test whether the potent dexamethasone effect was due to dual action in

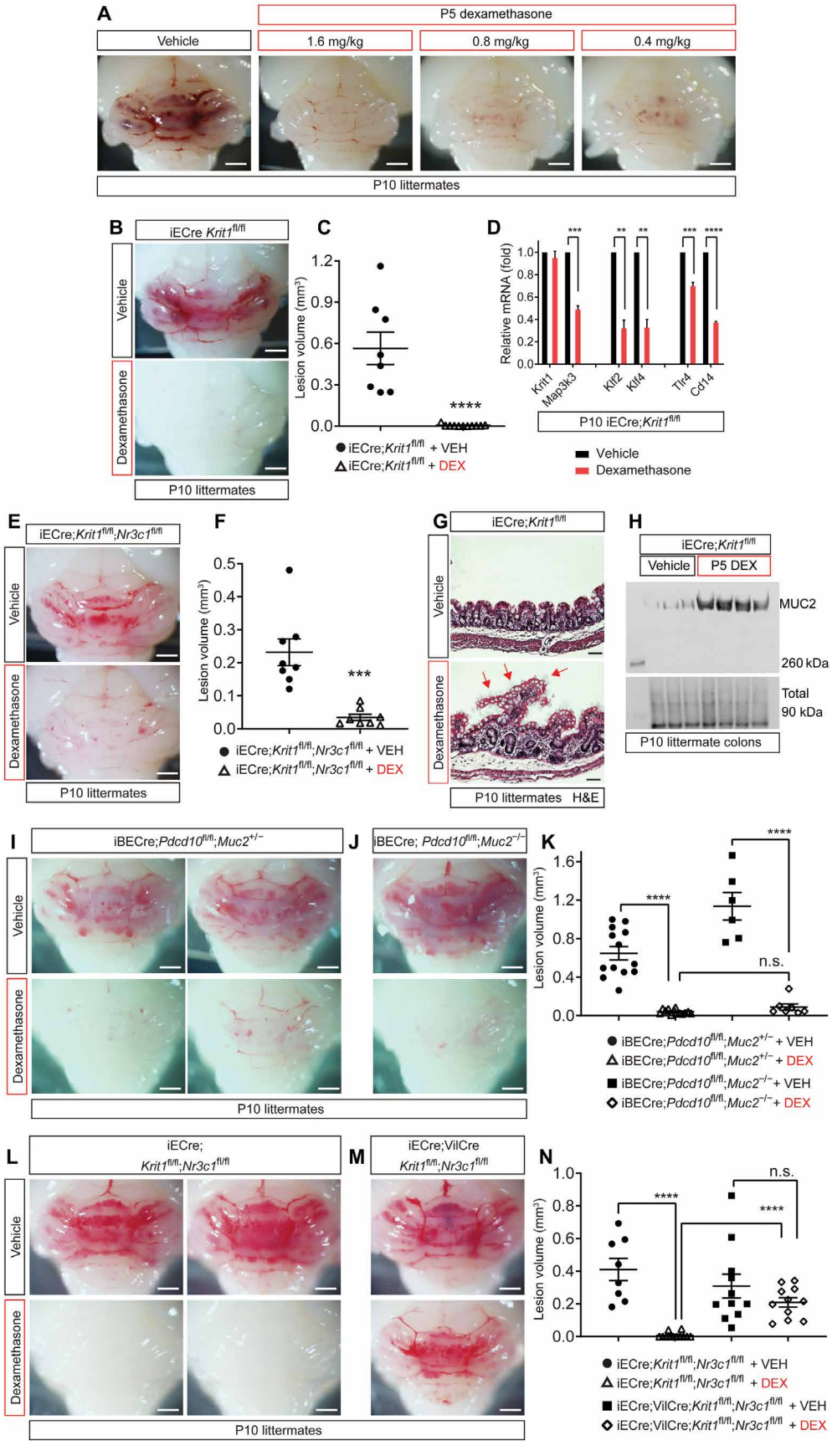

Fig. 8. Demonstration of a therapeutic gut-brain axis using dexamethasone. (**A**) Visual assessment of CCM formation in 10-day-old (P10) iECre;*Krit1*$^{fl/fl}$ littermates treated at P5 with vehicle or the indicated doses of dexamethasone. A dose of 0.8 mg/kg was used for all following experiments. Scale bars, 1 mm. Images are representative of $n \geq 3$ animals per treatment group from at least 2 distinct litters. (**B**) Visual assessment of CCM formation in iECre;*Krit1*$^{fl/fl}$ littermates treated with vehicle or dexamethasone. Scale bars, 1 mm. (**C**) Blinded microCT quantitation of CCM lesion burden in P10 iCre;*Krit1*$^{fl/fl}$ littermates treated with vehicle or dexamethasone. $n \geq 8$ animals per treatment group and 3 distinct litters. (**D**) Relative amounts of *Krit1*, *Map3k3*, *Klf2*, *Klf4*, *Tlr4*, and *Cd14* expression in cerebellar endothelial cells freshly isolated from P10 iECre;*Krit1*$^{fl/fl}$ littermates treated with P5 vehicle or dexamethasone. $n \geq 4$ animals per treatment group and 3 distinct litters. (**E**) Visual assessment of CCM formation in iECre;*Krit1*$^{fl/fl}$;*Nr3c1*$^{fl/fl}$ littermates treated with vehicle or dexamethasone. Scale bars, 1 mm. Results are representative of $n \geq 5$ animals per group and 5 independent experiments. (**F**) Blinded microCT quantitation of CCM lesion burden in P10 iECre;*Krit1*$^{fl/fl}$;*Nr3c1*$^{fl/fl}$ littermates treated with vehicle or dexamethasone. $n \geq 8$ animals per treatment group and 3 distinct litters. (**G**) H&E staining of P10 colon sections from iECre;*Krit1*$^{fl/fl}$ littermates treated with P5 vehicle or dexamethasone. Note the goblet cells in the dexamethasone-treated colon (arrows). Scale bars, 50 μm. (**H**) Immunoblot analysis of MUC2 expression in P10 colons from iECre;*Krit1*$^{fl/fl}$ littermates treated with P5 vehicle or dexamethasone (top; anti-MUC2). Total protein loading detected using REVERT is shown below. Molecular weight markers (in kilodalton) on left. Each lane is whole colonic lysate from one distinct animal. Results are representative of $n \geq 5$ animals per group and 2 distinct litters. (**I** and **J**) Visual assessment of CCM formation in iBECre;*Pdcd10*$^{fl/fl}$;*Muc2*$^{+/-}$ (I) and iBECre;*Pdcd10*$^{fl/fl}$;*Muc2*$^{-/-}$ (J) animals treated with P5 vehicle or dexamethasone. Scale bars, 1 mm. (**K**) Blinded microCT quantitation of CCM lesion burden in P10 iBECre;*Pdcd10*$^{fl/fl}$;*Muc2*$^{+/-}$ and iBECre;*Pdcd10*$^{fl/fl}$;*Muc2*$^{-/-}$ littermates treated with vehicle or dexamethasone. $n \geq 6$ animals per treatment group and ≥3 distinct litters. (**L** and **M**) Visual assessment of CCM formation in iECre;*Krit1*$^{fl/fl}$;*Nr3c1*$^{fl/fl}$ (L) and iECre;VilCre;*Krit1*$^{fl/fl}$;*Nr3c1*$^{fl/fl}$ (M) littermates at P10 after treatment with P5 vehicle or dexamethasone. Scale bars, 1 mm. (**N**) Blinded microCT quantitation of CCM lesion burden in P10 iECre;*Krit1*$^{fl/fl}$;*Nr3c1*$^{fl/fl}$ and iECre;VilCre;*Krit1*$^{fl/fl}$;*Nr3c1*$^{fl/fl}$ littermates treated with vehicle or dexamethasone. $n \geq 8$ animals per treatment group and 3 distinct litters. Error bars are shown as SEM, and significance is determined by unpaired, two-tailed Student's *t* test. $^{****}P < 0.0001$, $^{***}P < 0.001$, $^{**}P < 0.01$.

both brain endothelial cells and IECs, we next examined dexamethasone rescue in iECre;*Krit1*$^{fl/fl}$;*Nr3c1*$^{fl/fl}$ animals lacking GR only in endothelial cells and in littermate iECre;VilCre;*Krit1*$^{fl/fl}$;*Nr3c1*$^{fl/fl}$ animals lacking GR in both endothelial cells and IECs. iECre;*Krit1*$^{fl/fl}$;*Nr3c1*$^{fl/fl}$ animals treated with dexamethasone failed to develop CCMs (Fig. 8L), but dexamethasone-treated iECre;VilCre;*Krit1*$^{fl/fl}$;*Nr3c1*$^{fl/fl}$ animals developed robust lesion formation similar to those given vehicle only (Fig. 8, M and N). Although we cannot exclude effects of dexamethasone on the gut microbiome, effects of dexamethasone on other cell types such as immune cells, or the possibility that rescue is mediated solely by GR signaling in IECs, the potent ability of dexamethasone to block CCM formation is most readily explained by dual effects on brain endothelial cell signaling and IEC gut barrier formation. These studies suggest that pharmacologic targeting of multiple sites in a gut-brain axis disease mechanism may yield powerful therapeutic strategies (fig. S15, K and L).

DISCUSSION

A central molecular component of the gut-brain axis in CCM disease identified by these studies is the colonic mucus barrier that physically separates GNB in the colon from the epithelial cell layer and underlying blood vessels of the host. Loss of *Pdcd10* in gut epithelial cells resulted in a dose-dependent reduction in the thickness of the colonic mucus layer that correlated with an increase in CCM lesion formation. The changes in mucus layer thickness and CCM formation conferred by loss of IEC *Pdcd10* were replicated by dose-dependent loss of *Muc2*. A causal relationship between IEC *Pdcd10* and formation of the mucus barrier was further supported by nearly identical changes in gut microbial taxa abundance observed upon loss of *Pdcd10* or *Muc2*. These findings suggested that PDCD10 regulation of mucus production by goblet cells was a likely mechanism for its role in gut epithelial cells in CCM disease. Histologic analysis of the VilCre;*Pdcd10*$^{fl/fl}$ colon revealed abnormal, swollen goblet cells that contained large amounts of mucin despite the loss of the extraepithelial mucus barrier. Moreover, quantitative polymerase chain reaction and Western blot analysis of colonic epithelium demonstrated preserved total MUC2 mRNA and protein content in the colons of VilCre;*Pdcd10*$^{fl/+}$ and VilCre;*Pdcd10*$^{fl/fl}$ animals. Together, these findings are consistent with a requirement for PDCD10 during mucus secretion rather than MUC2 expression.

Our findings provide an explanation for the clinical observation that germline haploinsufficiency of *PDCD10* confers a more aggressive disease phenotype than germline haploinsufficiency of *KRIT1* or *CCM2*. Furthermore, they suggest that PDCD10 functions independently of the CCM complex in gut epithelial cells. Consistent with this observation, we found that gut epithelial loss of MEKK3, the kinase regulated by the CCM complex to prevent CCM formation by brain endothelial cells, also does not result in any change in the gut barrier. How does PDCD10 function to regulate the gut barrier? PDCD10 is a component of striatin-interacting phosphatase and kinase (STRIPAK) complexes that do not include KRIT1 or CCM2 and are not known to target MEKK3 (*49*). Moreover, PDCD10 has recently been found to participate in vesicle exocytosis in mammalian cells (*50*, *51*) and vesicle trafficking in *Caenorhabditis elegans* (*52*). Thus, although future studies are required to fully define the role of PDCD10 in gut epithelial cells, a mechanism in which PDCD10 functions as part of the STRIPAK but not CCM complex to regulate mucin secretion by goblet cells seems likely.

We acknowledge three main limitations regarding these findings. First, we cannot exclude the possibility that unique PDCD10 signaling in endothelial cells contributes to increased disease severity, although we demonstrated that the primary mechanism of lesion formation is gain of brain endothelial MEKK3 signaling (*51*). Second, although we showed in a variety of contexts that the gut barrier can affect CCM severity independently of the gut microbiome, these entities are so complex and intertwined that precisely parsing their individual effects is difficult. Third, this study was performed in mouse models; therefore, translation to human disease remains unproven. Our study illustrates the need to consider both the gut microbiome and barrier when assessing CCM disease risk in patients.

Can our findings be translated to improve the treatment and management of patients with CCM? First, proposed pharmacologic therapies for CCM disease must consider potential effects on gut barrier function. Drugs that adversely affect the gut barrier would be contraindicated, particularly as a chronic, lifelong therapy. Second, our studies of *Pdcd10*$^{+/-}$ animals with oral P80 intake confirm prior reports that such agents can reduce the colonic mucus barrier and suggest that common dietary factors such as emulsifiers in processed foods may have a relevant impact on CCM disease course through deleterious effects on the gut barrier. Third, exacerbation of CCM formation by DSS, commonly used to model inflammatory bowel disease in mice, suggests that gastrointestinal conditions associated with chronic inflammation, such as inflammatory bowel disease, are likely to accelerate CCM formation through effects on the gut barrier. Conversely, conditions that increase mucus production and/or reduce gut inflammation would be predicted to slow CCM disease progression.

Last, defining a gut-brain disease axis at the molecular and cellular levels enables the design of therapies to treat diseases refractory to conventional, "on-site" strategies. We have modeled such a therapeutic approach through analysis of an unexpectedly potent glucocorticoid treatment for CCM disease in mice. Genetic dissection of the dexamethasone mechanism of action to prevent CCM formation revealed that the drug acted through GRs in two cell types: brain endothelium and gut epithelium. Thus, the basis for dexamethasone's potency was most likely the fact that it targeted multiple key molecular and cellular mechanisms in the CCM gut-brain axis. Analogous single or multiple drug strategies designed to disable well-defined gut-brain axes may yield potent therapeutic strategies for other such pathologies in the future.

MATERIALS AND METHODS

Study design

As previously described (*20*), our lab has extensive experience with the P10 neonatal CCM mouse model. Sample sizes were estimated on the basis of our previous experience with the neonatal CCM model and lesion volume quantitation by blinded microCT, and our sample size calculations were previously detailed. Briefly, at P10, seven animals in each group would be expected to sufficiently power a study at 80% ($\beta = 0.2$) at a significance level of $\alpha = 0.05$, assuming an expected effect size of 80%, equal SDs, and normal distributions. For the P21 neonatal CCM model, we collected 20 brains at P21 and calculated a mean of 0.4 and an SD of 0.2. On the basis of our initial experience with DSS colitis in Fig. 2 (C and D), we assumed an effect size of 50%. Thus, each group would require 16 animals to power a study at 80% ($\beta = 0.2$) with a significance level of $\alpha = 0.05$, assuming equal SDs and normal

distributions. No data inclusion/exclusion or end point criteria were predefined or applied. No outliers were defined or excluded. Each experiment was performed at least twice with different litters and n greater than or equal to three (see specifics in each figure legend).

Research objectives were to define the role of the gut barrier in CCM severity using genetically engineered mouse models. We hypothesized that defects in the gut barrier would increase disease severity and that the clinical aggressiveness of *PDCD10* familial disease is caused by defects in gut barrier due to a unique role for PDCD10 in the intestinal epithelium. Research subjects included human patients with CCM and primarily genetically engineered mouse models. All experimental and control animals were littermates, and none were excluded from analysis at the time of harvest. Experimental animals were lost or excluded at two predefined points: (i) failure to properly inject 4-hydroxytamoxifen (4OHT) and observation of substantial leakage and (ii) death before P10 or P21 due to 4OHT injection or drug administration or other unknown causes. Given the early time points before weaning or sexual maturity, no attempt was made to distinguish or segregate results based on gender. Prior studies have found that adult animals heterozygous for CCM genes did not exhibit any difference in lesion burden with respect to gender (*53*, *54*), so no attempt was made to distinguish genders of animals used in adult CCM experiments.

Blinding was performed at multiple points during the experiments. Induction of the neonatal disease model was performed at 1 day of birth without knowledge of genotypes. MicroCT lesion volume quantification was performed in a blinded manner by investigators without knowledge of experimental details. 16*S* rRNA gene sequencing of both mouse and human samples were performed in blinded fashion until final analysis.

Statistics

As indicated in the specific figure legends, the SEM, 95% confidence interval, or boxplot is shown. Column data for each experiment were subjected to D'Agostino-Pearson normality tests, and only the P80 emulsifier experiments did not satisfy this test. We also found that in almost all experiments, the variance between groups was significantly ($P < 0.05$) different. Accordingly, we used unpaired, two-tailed, Welch's t tests for all two-group analyses, Kruskal-Wallis (nonparametric) one-way analysis of variance (ANOVA) with Dunn's correction for multiple comparisons in multiple-group analyses, or Mann-Whitney nonparametric U tests for experiments that did not satisfy normality tests. Because the Welch's t test underperforms on small sample sizes and variance calculations are meaningless for smaller samples, experiments with groups less than or equal to 10 distinct samples were analyzed using the unpaired, two-tailed Student's t test or one-way ANOVA with Holm-Sidak correction for multiple comparisons. Statistical tests for 16*S* rRNA gene sequencing analyses are detailed in the prior methods sections, and all significance ($P < 0.05$ or $q < 0.05$) tests were corrected for multiple comparisons using Bonferroni or Benjamini-Hochberg methods.

SUPPLEMENTARY MATERIALS

stm.sciencemag.org/cgi/content/full/11/520/eaaw3521/DC1

Materials and Methods

Fig. S1. PDCD10 deficiency in brain endothelial cell signaling in mice and the gut microbiome in humans compared to KRIT1 and CCM2.

Fig. S2. Single-cell RNA sequencing of the intestinal epithelium shows broad expression of *Krit1*, *Ccm2*, and *Pdcd10* across cell types.

Fig. S3. Analysis of the hindbrain upon deletion of *Pdcd10* solely in IECs.

Fig. S4. Quantification of the colonic mucus layer.

Fig. S5. Gut epithelial loss of CCM2 or MAP3K3 and subsequent effects on the colonic mucus barrier and fecal LCN2.

Fig. S6. Measurement of *Krit1*, *Ccm2*, and *Pdcd10* mRNA in the colonic epithelium.

Fig. S7. Analysis of goblet cell numbers, MUC2 expression, and colonic crypt morphology after intestine epithelial deletion of *Krit1*, *Ccm2*, or *Pdcd10*.

Fig. S8. E-cadherin (CDH1) expression and localization in colons lacking PDCD10, KRIT1, or MUC2.

Fig. S9. EpCAM expression and localization in colons lacking PDCD10, KRIT1, or MUC2.

Fig. S10. Intestinal junctions in PDCD10-deficient embryonic zebrafish.

Fig. S11. Heatmaps of 16*S* rRNA bacterial gene sequencing results for each animal by cage/litter.

Fig. S12. Unweighted principal component plots of 16*S* rRNA bacterial gene sequencing.

Fig. S13. Relative abundance boxplots of changed bacterial taxa as detected by 16*S* rRNA bacterial gene sequencing.

Fig. S14. Heatmaps of 16*S* rRNA bacterial gene sequencing results for the P80 emulsifier experiment by treatment group and cage.

Fig. S15. Dexamethasone effects on CCMs and colonic goblet cells.

Fig. S16. Model of the role of PDCD10 in the gut epithelium and its effect on CCM formation in the brain.

Table S1. Clinical characteristics of patients with CCM recruited to participate in gut microbiome study.

Data file S1. Raw data.

References (*55*–*69*)

View/request a protocol for this paper from *Bio-protocol*.

REFERENCES AND NOTES

1. C. Benakis, D. Brea, S. Caballero, G. Faraco, J. Moore, M. Murphy, G. Sita, G. Racchumi, L. Ling, E. G. Pamer, C. Iadecola, J. Anrather, Commensal microbiota affects ischemic stroke outcome by regulating intestinal γδ T cells. *Nat. Med.* **22**, 516–523 (2016).
2. D. Stanley, L. J. Mason, K. E. Mackin, Y. N. Srikhanta, D. Lyras, M. D. Prakash, K. Nurgali, A. Venegas, M. D. Hill, R. J. Moore, C. H. Wong, Translocation and dissemination of commensal bacteria in post-stroke infection. *Nat. Med.* **22**, 1277–1284 (2016).
3. G. Faraco, D. Brea, L. Garcia-Bonilla, G. Wang, G. Racchumi, H. Chang, I. Buendia, M. M. Santisteban, S. G. Segarra, K. Koizumi, Y. Sugiyama, M. Murphy, H. Voss, J. Anrather, C. Iadecola, Dietary salt promotes neurovascular and cognitive dysfunction through a gut-initiated TH17 response. *Nat. Neurosci.* **21**, 240–249 (2018).
4. T. R. Sampson, J. W. Debelius, T. Thron, S. Janssen, G. G. Shastri, Z. E. Ilhan, C. Challis, C. E. Schretter, S. Rocha, V. Gradinaru, M. F. Chesselet, A. Keshavarzian, K. M. Shannon, R. Krajmalnik-Brown, P. Wittung-Stafshede, R. Knight, S. K. Mazmanian, Gut microbiota regulate motor deficits and neuroinflammation in a model of Parkinson's disease. *Cell* **167**, 1469–1480.e12 (2016).
5. P. Y. Wang, L. Caspi, C. K. Lam, M. Chari, X. Li, P. E. Light, R. Gutierrez-Juarez, M. Ang, G. J. Schwartz, T. K. Lam, Upper intestinal lipids trigger a gut–brain–liver axis to regulate glucose production. *Nature* **452**, 1012–1016 (2008).
6. R. J. Perry, L. Peng, N. A. Barry, G. W. Cline, D. Zhang, R. L. Cardone, K. F. Petersen, R. G. Kibbey, A. L. Goodman, G. I. Shulman, Acetate mediates a microbiome–brain–β-cell axis to promote metabolic syndrome. *Nature* **534**, 213–217 (2016).
7. B. L. Bonaz, C. N. Bernstein, Brain-gut interactions in inflammatory bowel disease. *Gastroenterology* **144**, 36–49 (2013).
8. G. Sharon, N. Garg, J. Debelius, R. Knight, P. C. Dorrestein, S. K. Mazmanian, Specialized metabolites from the microbiome in health and disease. *Cell Metab.* **20**, 719–730 (2014).
9. T. C. Fung, C. A. Olson, E. Y. Hsiao, Interactions between the microbiota, immune and nervous systems in health and disease. *Nat. Neurosci.* **20**, 145–155 (2017).
10. I. Spadoni, G. Fornasa, M. Rescigno, Organ-specific protection mediated by cooperation between vascular and epithelial barriers. *Nat. Rev. Immunol.* **17**, 761–773 (2017).
11. S. Spiegler, M. Rath, C. Paperlein, U. Felbor, Cerebral cavernous malformations: An update on prevalence, molecular genetic analyses, and genetic counselling. *Mol. Syndromol.* **9**, 60–69 (2018).
12. A. Akers, R. Al-Shahi Salman, I. A. Awad, K. Dahlem, K. Flemming, B. Hart, H. Kim, I. Jusue-Torres, D. Kondziolka, C. Lee, L. Morrison, D. Rigamonti, T. Rebeiz, E. Tournier-Lasserve, D. Waggoner, K. Whitehead, Synopsis of guidelines for the clinical management of cerebral cavernous malformations: Consensus recommendations based on systematic literature review by the angioma alliance scientific advisory board clinical experts panel. *Neurosurgery* **80**, 665–680 (2017).
13. Z. Zhou, A. T. Tang, W.-Y. Wong, S. Bamezai, L. M. Goddard, R. Shenkar, S. Zhou, J. Yang, A. C. Wright, M. Foley, J. S. Arthur, K. J. Whitehead, I. A. Awad, D. Y. Li, X. Zheng, M. L. Kahn, Cerebral cavernous malformations arise from endothelial gain of MEKK3–KLF2/4 signalling. *Nature* **532**, 122–126 (2016).
14. O. S. Fisher, H. Deng, D. Liu, Y. Zhang, R. Wei, Y. Deng, F. Zhang, A. Louvi, B. E. Turk, T. J. Boggon, B. Su, Structure and vascular function of MEKK3–cerebral cavernous malformations 2 complex. *Nat. Commun.* **6**, 7937 (2015).

15. X. Wang, Y. Hou, K. Deng, Y. Zhang, D.-C. Wang, J. Ding, Structural insights into the molecular recognition between cerebral cavernous malformation 2 and mitogen-activated protein kinase kinase kinase 3. *Structure* **23**, 1087–1096 (2015).
16. X. Cullere, E. Plovie, P. M. Bennett, C. A. MacRae, T. N. Mayadas, The cerebral cavernous malformation proteins CCM2L and CCM2 prevent the activation of the MAP kinase MEKK3. *Proc. Natl. Acad. Sci. U.S.A.* **112**, 14284–14289 (2015).
17. Z. Zhou, D. R. Rawnsley, L. M. Goddard, W. Pan, X. J. Cao, Z. Jakus, H. Zheng, J. Yang, J. S. Arthur, K. J. Whitehead, D. Li, B. Zhou, B. A. Garcia, X. Zheng, M. L. Kahn, The cerebral cavernous malformation pathway controls cardiac development via regulation of endocardial MEKK3 signaling and KLF expression. *Dev. Cell* **32**, 168–180 (2015).
18. C. Denier, P. Labauge, F. Bergametti, F. Marchelli, F. Riant, M. Arnoult, J. Maciazek, E. Vicaut, L. Brunereau, E. Tournier-Lasserve, Genotype–phenotype correlations in cerebral cavernous malformations patients. *Ann. Neurol.* **60**, 550–556 (2006).
19. R. Shenkar, C. Shi, T. Rebeiz, R. A. Stockton, D. A. McDonald, A. G. Mikati, L. Zhang, C. Austin, A. L. Akers, C. J. Gallione, A. Rorrer, M. Gunel, W. Min, J. Marcondes de Souza, C. Lee, D. A. Marchuk, I. A. Awad, Exceptional aggressiveness of cerebral cavernous malformation disease associated with PDCD10 mutations. *Genet. Med.* **17**, 188–196 (2015).
20. A. T. Tang, J. P. Choi, J. J. Kotzin, Y. Yang, C. C. Hong, N. Hobson, R. Girard, H. A. Zeineddine, R. Lightle, T. Moore, Y. Cao, R. Shenkar, M. Chen, P. Mericko, J. Yang, L. Li, C. Tanes, D. Kobuley, U. Võsa, K. J. Whitehead, D. Y. Li, L. Franke, B. Hart, M. Schwaninger, J. Henao-Mejia, L. Morrison, H. Kim, I. A. Awad, X. Zheng, M. L. Kahn, Endothelial TLR4 and the microbiome drive cerebral cavernous malformations. *Nature* **545**, 305–310 (2017).
21. A. L. Akers, E. Johnson, G. K. Steinberg, J. M. Zabramski, D. A. Marchuk, Biallelic somatic and germline mutations in cerebral cavernous malformations (CCMs): Evidence for a two-hit mechanism of CCM pathogenesis. *Hum. Mol. Genet.* **18**, 919–930 (2009).
22. J. S. Zawistowski, L. Stalheim, M. T. Uhlik, A. N. Abell, B. B. Ancrile, G. L. Johnson, D. A. Marchuk, CCM1 and CCM2 protein interactions in cell signaling: Implications for cerebral cavernous malformations pathogenesis. *Hum. Mol. Genet.* **14**, 2521–2531 (2005).
23. D. A. Ridder, M.-F. Lang, S. Salinin, J.-P. Röderer, M. Struss, C. Maser-Gluth, M. Schwaninger, TAK1 in brain endothelial cells mediates fever and lethargy. *J. Exp. Med.* **208**, 2615–2623 (2011).
24. R. Cuttano, N. Rudini, L. Bravi, M. Corada, C. Giampietro, E. Papa, M. F. Morini, L. Maddaluno, N. Baeyens, R. H. Adams, M. K. Jain, G. K. Owens, M. Schwartz, M. G. Lampugnani, E. Dejana, KLF4 is a key determinant in the development and progression of cerebral cavernous malformations. *EMBO Mol. Med.* **8**, 6–24 (2016).
25. M. Renz, C. Otten, E. Faurobert, F. Rudolph, Y. Zhu, G. Boulday, J. Duchene, M. Mickoleit, A. C. Dietrich, C. Ramspacher, E. Steed, S. Manet-Dupé, A. Benz, D. Hassel, J. Vermot, J. Huisken, E. Tournier-Lasserve, U. Felbor, U. Sure, C. Albiges-Rizo, S. Abdelilah-Seyfried, Regulation of β1 integrin-Klf2-mediated angiogenesis by CCM proteins. *Dev. Cell* **32**, 181–190 (2015).
26. J. P. Choi, M. Foley, Z. Zhou, W.-Y. Wong, N. Gokoolparsadh, J. S. Arthur, D. Y. Li, X. Zheng, Micro-CT imaging reveals Mekk3 heterozygosity prevents cerebral cavernous malformations in Ccm2-deficient mice. *PLOS ONE* **11**, e0160833 (2016).
27. R. Girard, H. A. Zeineddine, C. Orsbon, H. Tan, T. Moore, N. Hobson, R. Shenkar, R. Lightle, C. Shi, M. D. Fam, Y. Cao, L. Shen, A. I. Neander, A. Rorrer, C. Gallione, A. T. Tang, M. L. Kahn, D. A. Marchuk, Z. X. Luo, I. A. Awad, Micro-computed tomography in murine models of cerebral cavernous malformations as a paradigm for brain disease. *J. Neurosci. Methods* **271**, 14–24 (2016).
28. G. D. Wu, J. Chen, C. Hoffmann, K. Bittinger, Y.-Y. Chen, S. A. Keilbaugh, M. Bewtra, D. Knights, W. A. Walters, R. Knight, R. Sinha, E. Gilroy, K. Gupta, R. Baldassano, L. Nessel, H. Li, F. D. Bushman, J. D. Lewis, Linking long-term dietary patterns with gut microbial enterotypes. *Science* **334**, 105–108 (2011).
29. D. Rothschild, O. Weissbrod, E. Barkan, A. Kurilshikov, T. Korem, D. Zeevi, P. I. Costea, A. Godneva, I. N. Kalka, N. Bar, S. Shilo, D. Lador, A. V. Vila, N. Zmora, M. Pevsner-Fischer, D. Israeli, N. Kosower, G. Malka, B. C. Wolf, T. Avnit-Sagi, M. Lotan-Pompan, A. Weinberger, Z. Halpern, S. Carmi, J. Fu, C. Wijmenga, A. Zhernakova, E. Elinav, E. Segal, Environment dominates over host genetics in shaping human gut microbiota. *Nature* **555**, 210–215 (2018).
30. H. A. Zeineddine, R. Girard, L. Saadat, L. Shen, R. Lightle, T. Moore, Y. Cao, N. Hobson, R. Shenkar, K. Avner, K. Chaudager, J. Koskimäki, S. P. Polster, M. D. Fam, C. Shi, M. A. Lopez-Ramirez, A. T. Tang, C. Gallione, M. L. Kahn, M. Ginsberg, D. A. Marchuk, I. A. Awad, Phenotypic characterization of murine models of cerebral cavernous malformations. *Lab. Invest.* **99**, 319–330 (2019).
31. M. E. Johansson, M. Phillipson, J. Petersson, A. Velcich, L. Holm, G. C. Hansson, The inner of the two Muc2 mucin-dependent mucus layers in colon is devoid of bacteria. *Proc. Natl. Acad. Sci. U.S.A.* **105**, 15064–15069 (2008).
32. M. E. Johansson, J. K. Gustafsson, K. E. Sjöberg, J. Petersson, L. Holm, H. Sjövall, G. C. Hansson, Bacteria penetrate the inner mucus layer before inflammation in the dextran sulfate colitis model. *PLOS ONE* **5**, e12238 (2010).
33. M. E. Johansson, J. M. Larsson, G. C. Hansson, The two mucus layers of colon are organized by the MUC2 mucin, whereas the outer layer is a legislator of host–microbial interactions. *Proc. Natl. Acad. Sci. U.S.A.* **108** (suppl. 1), 4659–4665 (2011).
34. B. Chassaing, G. Srinivasan, M. A. Delgado, A. N. Young, A. T. Gewirtz, M. Vijay-Kumar, Fecal lipocalin 2, a sensitive and broadly dynamic non-invasive biomarker for intestinal inflammation. *PLOS ONE* **7**, e44328 (2012).
35. K. S. Bergstrom, V. Kissoon-Singh, D. L. Gibson, C. Ma, M. Montero, H. P. Sham, N. Ryz, T. Huang, A. Velcich, B. B. Finlay, K. Chadee, B. A. Vallance, Muc2 protects against lethal infectious colitis by disassociating pathogenic and commensal bacteria from the colonic mucosa. *PLOS Pathog.* **6**, e1000902 (2010).
36. G. M. Birchenough, E. E. Nyström, M. E. Johansson, G. C. Hansson, A sentinel goblet cell guards the colonic crypt by triggering Nlrp6-dependent Muc2 secretion. *Science* **352**, 1535–1542 (2016).
37. M. Van der Sluis, B. A. De Koning, A. C. De Bruijn, A. Velcich, J. P. Meijerink, J. B. Van Goudoever, H. A. Büller, J. Dekker, I. Van Seuningen, I. B. Renes, A. W. Einerhand, Muc2-deficient mice spontaneously develop colitis, indicating that MUC2 is critical for colonic protection. *Gastroenterology* **131**, 117–129 (2006).
38. M. R. Schneider, M. Dahlhoff, D. Horst, B. Hirschi, K. Trülzsch, J. Müller-Höcker, R. Vogelmann, M. Allgäuer, M. Gerhard, S. Steininger, E. Wolf, F. T. Kolligs, A key role for E-cadherin in intestinal homeostasis and Paneth cell maturation. *PLOS ONE* **5**, e14325 (2010).
39. K. M. Draheim, O. S. Fisher, T. J. Boggon, D. A. Calderwood, Cerebral cavernous malformation proteins at a glance. *J. Cell Sci.* **127**, 701–707 (2014).
40. J. L. Sonnenburg, J. Xu, D. D. Leip, C.-H. Chen, B. P. Westover, J. Weatherford, J. D. Buhler, J. I. Gordon, Glycan foraging in vivo by an intestine-adapted bacterial symbiont. *Science* **307**, 1955–1959 (2005).
41. H. E. Jakobsson, A. M. Rodríguez-Piñeiro, A. Schütte, A. Ermund, P. Boysen, M. Bemark, F. Sommer, F. Bäckhed, G. C. Hansson, M. E. Johansson, The composition of the gut microbiota shapes the colon mucus barrier. *EMBO Rep.* **16**, 164–177 (2015).
42. M. Mamantopoulos, F. Ronchi, F. Van Hauwermeiren, S. Vieira-Silva, B. Yilmaz, L. Martens, Y. Saeys, S. K. Drexler, A. S. Yazdi, J. Raes, M. Lamkanfi, K. D. McCoy, A. Wullaert, Nlrp6- and ASC-dependent inflammasomes do not shape the commensal gut microbiota composition. *Immunity* **47**, 339–348.e4 (2017).
43. B. Chassaing, O. Koren, J. K. Goodrich, A. C. Poole, S. Srinivasan, R. E. Ley, A. T. Gewirtz, Dietary emulsifiers impact the mouse gut microbiota promoting colitis and metabolic syndrome. *Nature* **519**, 92–96 (2015).
44. S. J. Desmet, K. De Bosscher, Glucocorticoid receptors: Finding the middle ground. *J. Clin. Invest.* **127**, 1136–1145 (2017).
45. J. E. Goodwin, Y. Feng, H. Velazquez, W. C. Sessa, Endothelial glucocorticoid receptor is required for protection against sepsis. *Proc. Natl. Acad. Sci. U.S.A.* **110**, 306–311 (2013).
46. J. E. Goodwin, Y. Feng, H. Velazquez, H. Zhou, W. C. Sessa, Loss of the endothelial glucocorticoid receptor prevents the therapeutic protection afforded by dexamethasone after LPS. *PLOS ONE* **9**, e108126 (2014).
47. I. Das, C. W. Png, I. Oancea, S. Z. Hasnain, R. Lourie, M. Proctor, R. D. Eri, Y. Sheng, D. I. Crane, T. H. Florin, M. A. McGuckin, Glucocorticoids alleviate intestinal ER stress by enhancing protein folding and degradation of misfolded proteins. *J. Exp. Med.* **210**, 1201–1216 (2013).
48. D. E. Becker, Basic and clinical pharmacology of glucocorticosteroids. *Anesth. Prog.* **60**, 25–32 (2013).
49. M. Goudreault, L. M. D'Ambrosio, M. J. Kean, M. J. Mullin, B. G. Larsen, A. Sanchez, S. Chaudhry, G. I. Chen, F. Sicheri, A. I. Nesvizhskii, R. Aebersold, B. Raught, A.-C. Gingras, A PP2A phosphatase high density interaction network identifies a novel striatin-interacting phosphatase and kinase complex linked to the cerebral cavernous malformation 3 (CCM3) protein. *Mol. Cell. Proteomics* **8**, 157–171 (2009).
50. Y. Zhang, W. Tang, H. Zhang, X. Niu, Y. Xu, J. Zhang, K. Gao, W. Pan, T. J. Boggon, D. Toomre, W. Min, D. Wu, A network of interactions enables CCM3 and STK24 to coordinate UNC13D-driven vesicle exocytosis in neutrophils. *Dev. Cell* **27**, 215–226 (2013).
51. H. Jenny Zhou, L. Qin, H. Zhang, W. Tang, W. Ji, Y. He, X. Liang, Z. Wang, Q. Yuan, A. Vortmeyer, D. Toomre, G. Fuh, M. Yan, M. S. Kluger, D. Wu, W. Min, Endothelial exocytosis of angiopoietin-2 resulting from CCM3 deficiency contributes to cerebral cavernous malformation. *Nat. Med.* **22**, 1033–1042 (2016).
52. S. Pal, B. Lant, B. Yu, R. Tian, J. Tong, J. R. Krieger, M. F. Moran, A.-C. Gingras, W. B. Derry, CCM-3 promotes *C. elegans* germline development by regulating vesicle trafficking cytokinesis and polarity. *Curr. Biol.* **27**, 868–876 (2017).
53. D. A. McDonald, C. Shi, R. Shenkar, R. A. Stockton, F. Liu, M. H. Ginsberg, D. A. Marchuk, I. A. Awad, Fasudil decreases lesion burden in a murine model of cerebral cavernous malformation disease. *Stroke* **43**, 571–574 (2012).
54. R. Shenkar, C. Shi, C. Austin, T. Moore, R. Lightle, Y. Cao, L. Zhang, M. Wu, H. A. Zeineddine, R. Girard, D. A. McDonald, A. Rorrer, C. Gallione, P. Pytel, J. K. Liao, D. A. Marchuk, I. A. Awad, RhoA kinase inhibition with fasudil versus simvastatin in murine models of cerebral cavernous malformations. *Stroke* **48**, 187–194 (2017).

55. Y. Wang, M. Nakayama, M. E. Pitulescu, T. S. Schmidt, M. L. Bochenek, A. Sakakibara, S. Adams, A. Davy, U. Deutsch, U. Lüthi, A. Barberis, L. E. Benjamin, T. Mäkinen, C. D. Nobes, R. H. Adams, Ephrin-B2 controls VEGF-induced angiogenesis and lymphangiogenesis. *Nature* **465**, 483–486 (2010).
56. T. M. Mleynek, A. Chan, M. Redd, C. C. Gibson, C. Davis, D. S. Shi, T. Chen, K. L. Carter, J. Ling, R. Blanco, H. Gerhardt, K. Whitehead, D. Y. Li, Lack of CCM1 induces hypersprouting and impairs response to flow. *Hum. Mol. Genet.* **23**, 6223–6234 (2014).
57. X. Zheng, C. Xu, A. O. Smith, A. N. Stratman, Z. Zou, B. Kleaveland, L. Yuan, C. Didiku, A. Sen, X. Liu, N. Skuli, A. Zaslavsky, M. Chen, L. Cheng, G. E. Davis, M. L. Kahn, Dynamic regulation of the cerebral cavernous malformation pathway controls vascular stability and growth. *Dev. Cell* **23**, 342–355 (2012).
58. A. Velcich, W. Yang, J. Heyer, A. Fragale, C. Nicholas, S. Viani, R. Kucherlapati, M. Lipkin, K. Yang, L. Augenlicht, Colorectal cancer in mice genetically deficient in the mucin Muc2. *Science* **295**, 1726–1729 (2002).
59. B. B. Madison, L. Dunbar, X. T. Qiao, K. Braunstein, E. Braunstein, D. L. Gumucio, Cis elements of the villin gene control expression in restricted domains of the vertical (crypt) and horizontal (duodenum, cecum) axes of the intestine. *J. Biol. Chem.* **277**, 33275–33283 (2002).
60. P. R. Mittelstadt, J. P. Monteiro, J. D. Ashwell, Thymocyte responsiveness to endogenous glucocorticoids is required for immunological fitness. *J. Clin. Invest.* **122**, 2384–2394 (2012).
61. J. A. Gagnon, E. Valen, S. B. Thyme, P. Huang, L. Akhmetova, A. Pauli, T. G. Montague, S. Zimmerman, C. Richter, A. F. Schier, Efficient mutagenesis by Cas9 protein-mediated oligonucleotide insertion and large-scale assessment of single-guide RNAs. *PLOS ONE* **9**, e98186 (2014).
62. L.-E. Jao, S. R. Wente, W. Chen, Efficient multiplex biallelic zebrafish genome editing using a CRISPR nuclease system. *Proc. Natl. Acad. Sci. U.S.A.* **110**, 13904–13909 (2013).
63. R. N. Kettleborough, E. M. Busch-Nentwich, S. A. Harvey, C. M. Dooley, E. de Bruijn, F. van Eeden, I. Sealy, R. J. White, C. Herd, I. J. Nijman, F. Fényes, S. Mehroke, C. Scahill, R. Gibbons, N. Wali, S. Carruthers, A. Hall, J. Yen, E. Cuppen, D. L. Stemple, A systematic genome-wide analysis of zebrafish protein-coding gene function. *Nature* **496**, 494–497 (2013).
64. B. J. Callahan, P. J. McMurdie, M. J. Rosen, A. W. Han, A. J. Johnson, S. P. Holmes, DADA2: High-resolution sample inference from Illumina amplicon data. *Nat. Methods* **13**, 581–583 (2016).
65. D. McDonald, M. N. Price, J. Goodrich, E. P. Nawrocki, T. Z. DeSantis, A. Probst, G. L. Andersen, R. Knight, P. Hugenholtz, An improved Greengenes taxonomy with explicit ranks for ecological and evolutionary analyses of bacteria and archaea. *ISME J.* **6**, 610–618 (2012).
66. K. Katoh, D. M. Standley, MAFFT multiple sequence alignment software version 7: Improvements in performance and usability. *Mol. Biol. Evol.* **30**, 772–780 (2013).
67. M. N. Price, P. S. Dehal, A. P. Arkin, FastTree 2–Approximately maximum-likelihood trees for large alignments. *PLOS ONE* **5**, e9490 (2010).
68. C. Lozupone, R. Knight, UniFrac: A new phylogenetic method for comparing microbial communities. *Appl. Environ. Microbiol.* **71**, 8228–8235 (2005).
69. C. A. Lozupone, M. Hamady, S. T. Kelley, R. Knight, Quantitative and qualitative β diversity measures lead to different insights into factors that structure microbial communities. *Appl. Environ. Microbiol.* **73**, 1576–1585 (2007).

Acknowledgments: We thank the members of the Kahn lab and our colleagues J. Henao-Mejia, G. Wu, and R. Bushman for thoughtful comments and advice during this work. We thank Angioma Alliance for patient enrollment, the University of Chicago PaleoCT core facilities' expertise, and L. Guo for artwork. **Funding:** This work was supported by NIH grants R01HL094326 to M.L.K., P01NS092521 to M.L.K., D.A.M., and I.A.A., F30NS100252 to A.T.T., RO1CA174432 and R01CA229216 to L.A., R01HL136507 to W.M., and U54NS065705 to H.K. and L.M.; German DFG grant SCHW416/5-2 to M.S. and SE2016/7-2 and SE2016/10-1 to S.A.-S.; National Natural Science Foundation of China grants 81771240 to X.Z.; Australian National Health and Medical Research Council project grant APP1124011 to X.Z.; Excellence cluster REBIRTH SFB958 to S.A.-S.; a Penn-CHOP Microbiome Pilot and Feasibility Award grant to M.L.K.; and a Be Brave for Life Micro-Grant to M.L.K. Single-cell sequencing was supported by a grant from the State of Pennsylvania Health Research Formula Fund to C.J.L. MicroCT imaging was supported by University of Chicago Safadi Program of Excellence in Clinical and Translational Neuroscience Pilot Awards to L.S. and S.P.P. **Author contributions:** A.T.T. designed and performed most of the experiments and wrote the manuscript. K.R.S., C.C.H., L.M.G., A.M., and A.R. assisted in experiments. J.Y. and L.L. performed histologic analysis. R.G., T.M., R.L., N.H., R.S., L.S., S.P.P., and I.A.A. performed microCT CCM lesion imaging and quantification in a blinded manner. H.P., A.P., E.G., and D.A.M. performed experiments with the adult CCM model. C.T., L.M.M., and K.B. performed 16*S* rRNA gene sequencing and bioinformatics analysis on the mouse and human microbiome samples. C.J.R. and S.A.-S. performed zebrafish studies. A.T.T., P.M.-l., A.A., H.K., L.M., and I.A.A. organized and performed the CCM patient microbiome study. K.J.W., X.Z., A.V., L.A., M.S., and W.M. provided critical reagents. N.L., Q.Z., and C.J.L. performed single-cell sequencing experiments. M.L.K. designed experiments and wrote the manuscript. **Competing interests:** The authors declare that they have no competing financial interests. I.A.A. is Chairman of the Scientific Advisory Board for Angioma Alliance and provides expert opinions related to clinical care of CCMs. **Data and materials availability:** All data are present in the main text or in the Supplementary Materials. Transgenic mouse lines not available through public repositories are available from M.L.K. under a material transfer agreement with the University of Pennsylvania.

Submitted 14 December 2018
Resubmitted 17 July 2019
Accepted 9 October 2019
Published 27 November 2019
10.1126/scitranslmed.aaw3521

Citation: A. T. Tang, K. R. Sullivan, C. C. Hong, L. M. Goddard, A. Mahadevan, A. Ren, H. Pardo, A. Peiper, E. Griffin, C. Tanes, L. M. Mattei, J. Yang, L. Li, P. Mericko-Ishizuka, L. Shen, N. Hobson, R. Girard, R. Lightle, T. Moore, R. Shenkar, S. P. Polster, C. J. Roedel, N. Li, Q. Zhu, K. J. Whitehead, X. Zheng, A. Akers, L. Morrison, H. Kim, K. Bittinger, C. J. Lengner, M. Schwaninger, A. Velcich, L. Augenlicht, S. Abdelilah-Seyfried, W. Min, D. A. Marchuk, I. A. Awad, M. L. Kahn, Distinct cellular roles for PDCD10 define a gut-brain axis in cerebral cavernous malformation. *Sci. Transl. Med.* **11**, eaaw3521 (2019).

Science Translational Medicine

Distinct cellular roles for PDCD10 define a gut-brain axis in cerebral cavernous malformation

Alan T. Tang, Katie R. Sullivan, Courtney C. Hong, Lauren M. Goddard, Aparna Mahadevan, Aileen Ren, Heidy Pardo, Amy Peiper, Erin Griffin, Ceylan Tanes, Lisa M. Mattei, Jisheng Yang, Li Li, Patricia Mericko-Ishizuka, Le Shen, Nicholas Hobson, Romuald Girard, Rhonda Lightle, Thomas Moore, Robert Shenkar, Sean P. Polster, Claudia J. Roedel, Ning Li, Qin Zhu, Kevin J. Whitehead, Xiangjian Zheng, Amy Akers, Leslie Morrison, Helen Kim, Kyle Bittinger, Christopher J. Lengner, Markus Schwaninger, Anna Velcich, Leonard Augenlicht, Salim Abdelilah-Seyfried, Wang Min, Douglas A. Marchuk, Issam A. Awad and Mark L. Kahn

Sci Transl Med **11**, eaaw3521.
DOI: 10.1126/scitranslmed.aaw3521

Two effects in one gene

Cerebral cavernous malformation (CCM) is a genetic vascular disease affecting mainly the brain. Different genes can cause CCM and mutations in *PDCD10* are responsible for a particularly severe form of the disease. Now, Tang *et al.* show that modulation of the gut barrier could explain the poor prognosis of patients with *PDCD10* mutations. In mice, *Pdcd10* deletion specifically in the gut epithelium disrupted the colonic mucosal barrier and increased CCM formation. Pharmacologic experiments targeting the glucocorticoid system demonstrated that both brain endothelial cells and gut epithelial cells contribute to CCM formation, suggesting that therapies targeting either brain or gut signaling could be effective for treating CCM.